solution, permeabilized with 0.01% Triton X-100 and blocked in 1% BSA in PBS for 20 min at room temperature. Subsequent antibody incubations were in PBS containing 1% BSA–0.01% Triton X-100. Antibody reagents were mouse anti-α-tubulin (1:100, Sigma-Aldrich St. Louis, MO, USA) and rabbit anti-BMAL1 H-170 (1:200, Santa Cruz Biotechnology, CA. 95060, USA). Incubation with primary antibody was kept overnight at 4°C, followed by three washes with PBS solution. Secondary reagent with Alexa Flour® 488-cojugated goat antimouse IgG, goat antirabbit IgG (1:1,000, Molecular probes, Invitrogen, Eugene, OR 97402, USA) and Alexa Flour® 594-cojugated goat antimouse IgG (1:700, Molecular probes, Invitrogen Eugene, OR 97402, USA). Secondary antibodies were incubated for 1 hr at room temperature. After PBS washing, independent mounting was done with Prolong Gold antifade reagent supplemented with 4,6-diamidino-2-phenylindole (DAPI) (Invitrogen, Carlsbad, CA, USA). All stained cells were visualized by confocal Eclipse TE 2000-E microscope (Nikon, Tokyo, Japan) with 20×, 40× and 60× objectives.

Tumor specimens of patients with MPM

Sixteen resected MPM tissue specimens were obtained from patients diagnosed with MPM who underwent surgery at the Department of Thoracic Surgery, Nagoya University Hospital between 2005 and 2011. Eleven patients received neoadjuvant chemotherapy with pemetrexed and cisplatin, while one patient received adjuvant chemotherapy and radiotherapy. Fifteen specimens were obtained through extra-pleural pneumonectomy and one was obtained by pleurectomy. Diagnosis of mesothelioma was made based on clinical evaluation, histopathologic examination, and the clinical stage was determined according to the International Mesothelioma Interest Group.[18] Patients' overall survival was defined as the length of time from the date of surgery to that of death. Four noncancerous (normal parietal pleura) tissue specimens were obtained from patients who underwent thoracic surgery for different causes (*i.e.*, not including mesothelioma) and were used as normal controls. The study protocol was approved by the Institutional Review Boards of Nagoya University Graduate School of Medicine. Informed consent was obtained from the patients following institutional guidelines. The expression level of the circadian clock protein, *BMAL1*, was examined in the aforementioned surgically resected specimens. Sections from formalin-fixed paraffin-embedded were treated for immunostaining with commercially available BMAL1 antibody (Sanata Cruz Biotechnology, CA.95060, USA) according to the procedures described elsewhere.[13]

Cell growth assays

Colorimetric proliferation assay was performed using WST-1 assay kit (Roche, Basel, Switzerland) according to manufacturer's instruction. Liquid and soft agar colony formation assays were done as described previously.[19]

Cell cycle analysis

Post-transfection with *BMAL1*-siRNA or control oligos, cells were synchronized by serum starvation for 12 hr or by double-thymidine treatment (to block mitosis and induce late G1/early S phase arrest; subconfluent cell cultures were incubated in complete medium containing 2 mM thymidine for 18 hr, and then, the thymidine medium was removed and replaced with complete medium lacking thymidine for 12 hr followed by another 18-hr incubation in the presence of thymidine). Synchronized populations were harvested and washed in ice-cold PBS. Following centrifugation at 900*g* for 5 min, cells were suspended in 150 μL of cold PBS while vortex gently, and cells were fixed by dropwise addition of 350 μL ice-cold ethanol. Fixed cells were stored at −20°C for at least 30 min. For staining, pelleted cells were washed twice with cold PBS and resuspended in 0.5 mL PBS containing 200 μg/mL RNase, and stained with propidium iodide 20 μg. Cells were incubated at 37°C for 30 min and maintained at 4°C before analysis, cells were filtered through 40 μM nylon mesh and analyzed by flow cytometry for cell cycle status [FACS Calibur instrument (Becton Dickinson), with BD Cell Quest™ Pro Ver. 5.2.1 (BD) Bioscience, Franklin Lakes, NJ, USA].

Apoptosis analysis

Apoptosis was quantified by detecting surface exposure of phosphatidylserine in apoptotic cells using a phycoerythrin (PE)—Annexin V Apoptosis Detection Kit I (BD Biosciences). Cells were harvested 5 days after transfection of siRNA oligos, treated according to the manufacturer's instructions and measured with PE 7-amino-actinomycin D (7-AAD) staining using flow cytometry [FACS Calibur instrument (Becton Dickinson), with BD Cell Quest™ Pro Ver. 5.2.1 (BD) Bioscience, Franklin Lakes, NJ, USA].

Hematoxylin and eosin staining

Post-transfection with *BMAL1*-siRNA or control oligos, ACC-MESO-1 cells were harvested after 48 hr and 10,000 cells were plated/chambered in eight-well Lab-Tek™ Chamber Slide System, and then incubated overnight at 37°C and 5% CO_2. Next day, cells washed with PBS and fixed with 1% glutaraldehyde for 5 min and subsequently stained with Mayer's Hematoxylin solution (Muto Puro Chemical LTD, Tokyo, Japan) for 2–3 min, rinsed with distilled water and then submerged in Scott's tap water substitute (0.2% $NaHCO_3$ and 2% $MgSO_4$) for bluing, finally cells were washed with distilled water once and examined under the microscope.

Statistics

SPSS Ver. 18 software was used for all statistics analysis in this study. Mann–Whitney *U*-test was used for analyzing difference between two groups.

Results

MPM cell lines express higher levels of *BMAL1* than normal pleural mesothelial cells

Quantitative detection of *BMAL1* and *NPAS2* mRNA in a panel of MPM and MeT-5A cell lines was performed using qRT-PCR. Ten out of 13 (77%) MPM cell lines expressed

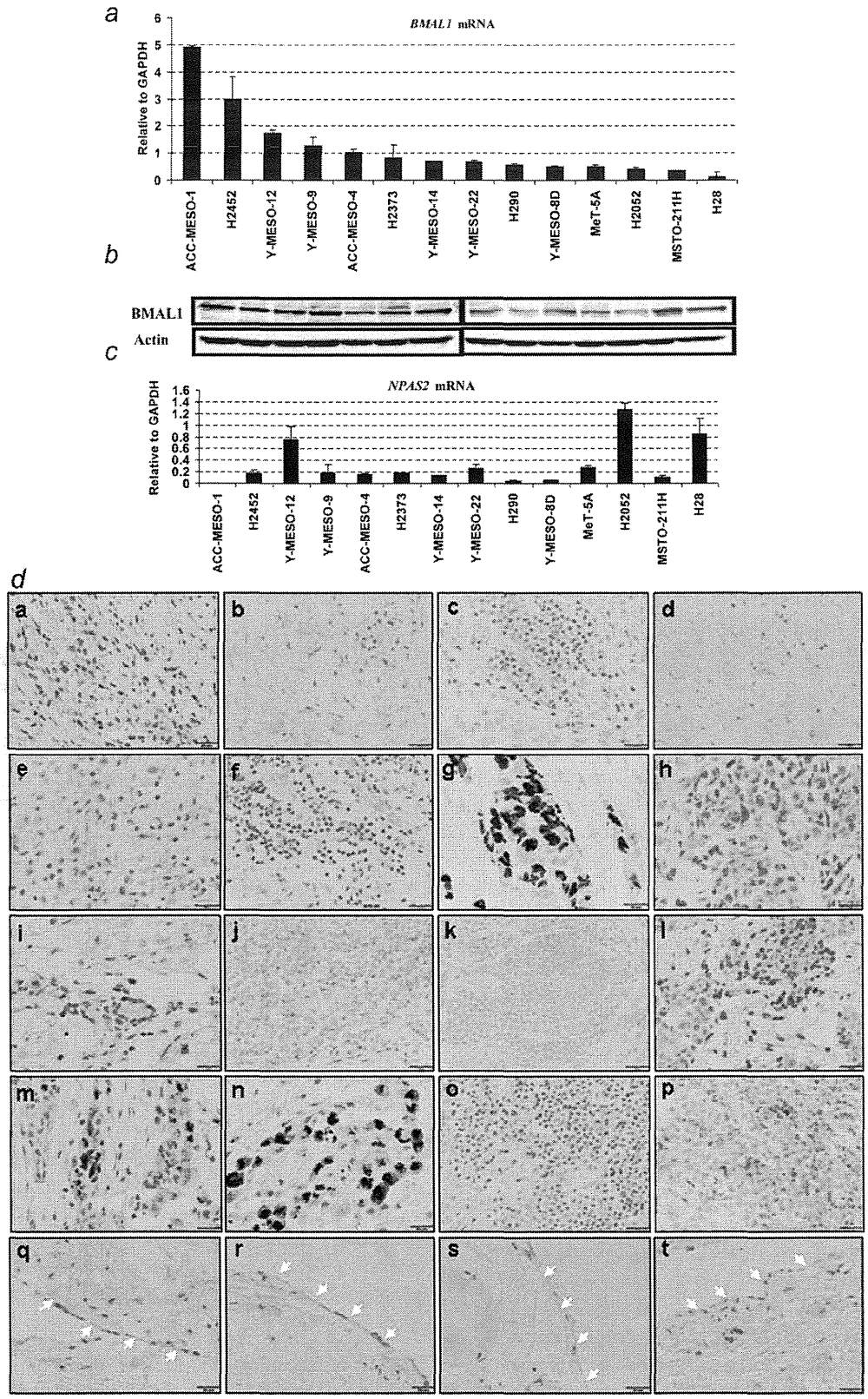

Figure 1. *BMAL1* expression levels in MPM and normal parietal pleura. (*a*) qRT-PCR analysis of *BMAL1* in 13 MPM cell lines and an immortalized pleural mesothelial cell line MeT-5A (control). The cell lines are aligned by expression levels of *BMAL1* mRNA from high (left) to low (right). The result is a representative of two independent qRT-PCR experiments done in duplicated reactions. (*b*) Western blots of *BMAL1* in MPM cell lines. Actin was used as a loading control. (*c*) qRT-PCR analysis of *NPAS2* in 13 MPM cell lines and MeT-5A. (*d*) Immunohistochemical staining of BMAL1 in surgically annotated MPM and normal parietal pleural specimens. Immunohistochemical analysis showed an overexpression of BMAL1 in a subset of MPM specimen (a–p), whereas normal pleural mesothelial cells showed negative BMAL1 immunoreactivity (white arrows, q–t). Details of MPM and normal parietal pleural specimens were mentioned in "Material and Methods" Section. ×400 magnification and 25 μm scale bars were used for all images. [Color figure can be viewed in the online issue, which is available at wileyonlinelibrary.com.]

Table 1. Clinical features of 16 patients with MPM

ID	Age/Sex	Histology	BMAL1 Status (IHC score)	Asbestos exposure	OS (M)	Staging		Surgery	Therapy
						Clinical	Pathological		
1	50/M	Biphasic	Negative (1+)	+	2.5	T2N0M0/II	T3N2M0/III	Right EPP	No
2	54/M	Biphasic	Negative (1+)	+	24.0	T2N0M0/II	T2N0M0/II	Left EPP	No
3	56/M	Epithelioid	Negative (1+)	+	25.3	T3N2M0/III	T4N0M0/IV	Left EPP	No
4	65/M	Epithelioid	Negative (0)	+	8.8	T3N1M0/III	T3N2M0/III	Right EPP	Neoadjuvant CT
5	46/F	Epithelioid	Negative (1+)	−	36.0	T1bN0M0/Ib	T3N2M0/III	Left EPP	Adjuvant CT + LRT
6	70/F	Epithelioid	Negative (0)	−	27.6	T1bN1M0/III	T2N1M0/III	Left EPP	Neoadjuvant CT
7	65/M	Epithelioid	Positive (3+)	+	8.4	T3N0M0/III	T4N0M0/IV	Right EPP	Neoadjuvant CT
8	60/M	Biphasic	Negative (0)	+	31.3	T3N2M0/III	T3N0M0/III	Right EPP	Neoadjuvant CT + PHR
9	62/M	Epithelioid	Positive (2+)	+	13.0	T3N0M0/III	T4NxM0/IV	Left pleurectomy	Neoadjuvant CT
10	67/M	Biphasic	Negative (1+)	−	11.6	T2N1M0/III	T3N0M0/III	Right EPP	Neoadjuvant CT + PHR
11	66/M	Biphasic	Negative (0)	+	8.3	T2N0M0/II	T3N0M0/III	Right EPP	Neoadjuvant CT
12	67/M	Epithelioid	Positive (2+)	+	3.6	T2N0M0/II	T3N2M0/III	Right EPP	No
13	68/M	Epithelioid	Positive (3+)	−	7.7	T3N0M0/III	T3N0M0/III	Left EPP	Neoadjuvant CT + PHR
14	63/M	Epithelioid	Positive (3+)	+	1.9	T2N0M0/II	T3N0M0/III	Lt EPP	Neoadjuvant CT
15	68/M	Sarcomatoid	Negative (0)	+	1.0	T3N2M0/III	T3N0M0/III	Right EPP	Neoadjuvant CT
16	64/M	Epithelioid	Negative (1+)	+	0.8	T2N0M0/II	T3N2M0/III	Left EPP	Neoadjuvant CT

Abbreviations: Id, patient's number; IHC, immunohistochemical score for *BMAL1*; OS, overall survival; M, month; EPP, extra-pleural pneumonectomy; neoadjuvant CT, neoadjuvant chemotherapy (cisplatin + pemetrexed); adjuvant chemotherapy (cisplatin + pemetrexed); LRT, local radiation therapy; PHR, post-operative hemithoracic radiation.

higher levels of *BMAL1* mRNA than MeT-5A, while *NPAS2* expression profile seems different from *BMAL1* profile in MPM cell lines (Figs. 1*a* and 1*c*). Western blot analysis for the same set of cell lines clearly demonstrated variable degrees of BMAL1 protein expression (Fig. 1*b*). Furthermore, we investigated *BMAL1* expression levels in 16 surgically annotated MPM and four normal parietal pleural specimens (Table 1). Through immunohistochemical analysis, BMAL1 was detected in a subset of MPM specimens with nuclear and/or cytoplasmic localization, while none of the four normal parietal pleural samples showed detectable levels of BMAL1 protein (Fig. 1*d*), suggesting that BMAL1 may be important in the development of MPM.

Expression profile of *BMAL1* and *CLOCK* over 24 hr in ACC-MESO-1 and MeT-5A cells

Based on previous data showing that expression of BMAL1 followed a rhythmical pattern in animal models,[20] we decided to examine the expression of *BMAL1* and *CLOCK* by qRT-PCR analysis to evaluate their oscillation over 24 hr in ACC-MESO-1 and MeT-5A cells. We used the mouse fibroblast cell line (NIH3T3) as a positive control as it shows a rhythmical expression of BMAL1.[20] Serum shock was done as described previously.[5] *BMAL1* rhythmical expression was found in serum-shocked normal nontumorigenic mesothelial cells but not in ACC-MESO-1 cells, whereas *CLOCK* showed rhythmical expression in both MPM and normal mesothelial cells (Fig. 2). These findings indicate that *BMAL1* rhythmical expression was intact in normal mesothelial cells but not in MPM cells.

BMAL1 knockdown suppresses proliferation, anchorage-dependent and independent clonal growth of MPM cells

To investigate the role of *BMAL1* in MPM cell growth, we performed RNAi-mediated gene silencing against *BMAL1*. ACC-MESO-1 and H290 cell lines were selected as the MPM cell models to be used for further investigations (Fig. 1*a*). MeT-5A was used as a normal control. To reduce the off target effects, we used low dose (10 nM) stealth selected RNAi (Invitrogen Carlsbad, CA, USA) which includes three siRNA oligos with nonoverlapping sequences targeting *BMAL1*. Efficient *BMAL1* knockdown was confirmed by qRT-PCR, western blotting and immunostaining (Fig. 3). Next, to evaluate the effect of *BMAL1* knockdown on cell proliferation in mass culture and clonogenic growth in anchorage-dependent and independent conditions, we performed colorimetric growth, liquid and soft agar colony formation assays. We found that in ACC-MESO-1 and H290 cells, *BMAL1* knockdown significantly suppressed proliferation and dramatically suppressed colony formation in anchorage-dependent (liquid colony formation assay) and anchorage-independent conditions (soft agar assay) (Fig. 4). By contrast, we did not see significant suppression of proliferation in MeT-5A (Supporting Information, Fig. S1*a*).

BMAL1 depletion induces massive apoptosis in MPM cells, with limited consequences in the normal pleural mesothelial cells

Next, we investigated whether the antiproliferative effect of *BMAL1* depletion is due to cell death. *BMAL1* knockdown resulted in massive apoptosis and necrosis in MPM cells (Fig. 5*a*), as evidenced by increases in cleaved caspase-3 activation

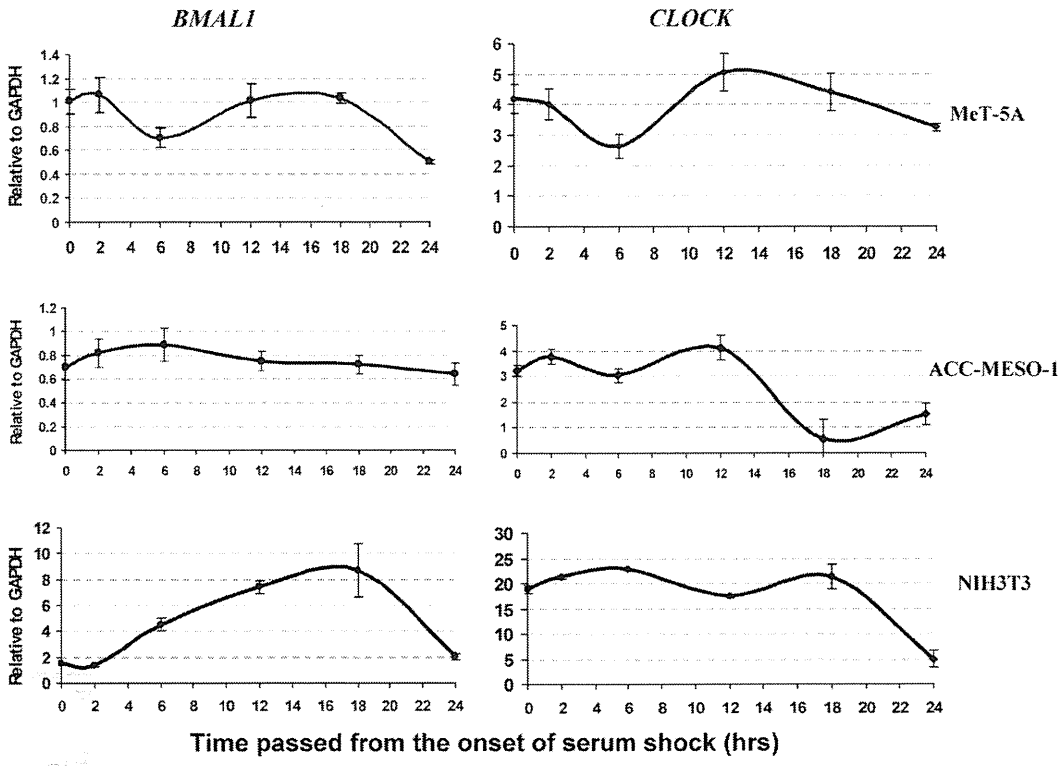

Figure 2. Expression profiles of *BMAL1* and *CLOCK* genes over 24 hr in ACC-MESO-1 and MeT-5A cells. qRT-PCR analysis of *BMAL1* and *CLOCK* mRNA in ACC-MESO-1, MeT-5A at time indicated above. NIH3T3 cells were used as a positive control. Serum shock was performed as mentioned in the "Materials and Methods" Section. We found that serum shock induces rhythmical expression changes of *BMAL1* and *CLOCK* mRNA in NIH3T3 as well as MeT-5A cells. Serum shocked ACC-MESO-1 cells showed rhythmical changes of *CLOCK* mRNA, but not *BMAL1* (GAPDH was used as an internal control). The results are averages of two independent experiments done in duplicate.

in ACC-MESO-1 cells (Fig. 5*b*). By contrast, subtle apoptosis could be found in MeT-5A cells following *BMAL1* knockdown (Fig. 5*a*). These results indicate that *BMAL1* knockdown-induced growth inhibition occurs in part through apoptotic mechanisms and MPM cells are more dependent on *BMAL1* expression for their survival than normal mesothelial cells.

BMAL1 knockdown leads to cell cycle disruption in ACC-MESO-1 cells with a clear rise of polyploidy

We investigated whether *BMAL1* knockdown-induced growth inhibition also was caused by cell cycle arrest. Consistent with induction of apoptosis as measured by cleaved caspase-3 expression, there was an increase in subG1 DNA content in ACC-MESO-1 transfected with *BMAL1*-siRNA oligos compared to cells transfected with control oligos (Fig. 5*c*). The proportion of cells in G1 phase decreased whereas a modest increase in the proportion of cells in G2/M phase. Notably, the profiling also showed an increase in the fraction of cells whose DNA contents exceed 4 *N* that correspond to polyploidy cell population. With much longer times in culture, high percentages of those cells (in G2/M phase and polyploidy region) decreased while subG1 population significantly increased (Fig. 5*c*), implying that polyploidy cells underwent apoptosis. By contrast, we did not see significant changes in cell cycle profiling of MeT-5A following *BMAL1* knockdown (Supporting Information, Fig. S1*b*).

Depletion of *BMAL1* induces drastic morphological alterations indicative of mitotic catastrophe in ACC-MESO-1 cells

We noted that following *BMAL1* knockdown, ACC-MESO-1 cells underwent drastic morphological changes; the cells enlarged and elongated by visual examination under phase contrast microscopy. Next, we performed hematoxlin and eosin (H–E) staining for these cells. As shown in Figure 6*a*, dramatic morphological alterations were seen in ACC-MESO-1 cells after *BMAL1* knockdown; cells exhibit much enlarged flattened shape, micronucleation, multiple nuclei and vacuolization occasionally were found. Next, we examined *BMAL1* siRNA-treated ACC-MESO-1 cells by detailed morphological analysis of DAPI-stained cell nuclei and α-tubulin immunostaining to visualize the cytoskeletal alterations associated with changes in nuclear morphology. Multiple morphological defects were identified which are consistent with the findings observed by H–E staining (Figs. 6*b* and

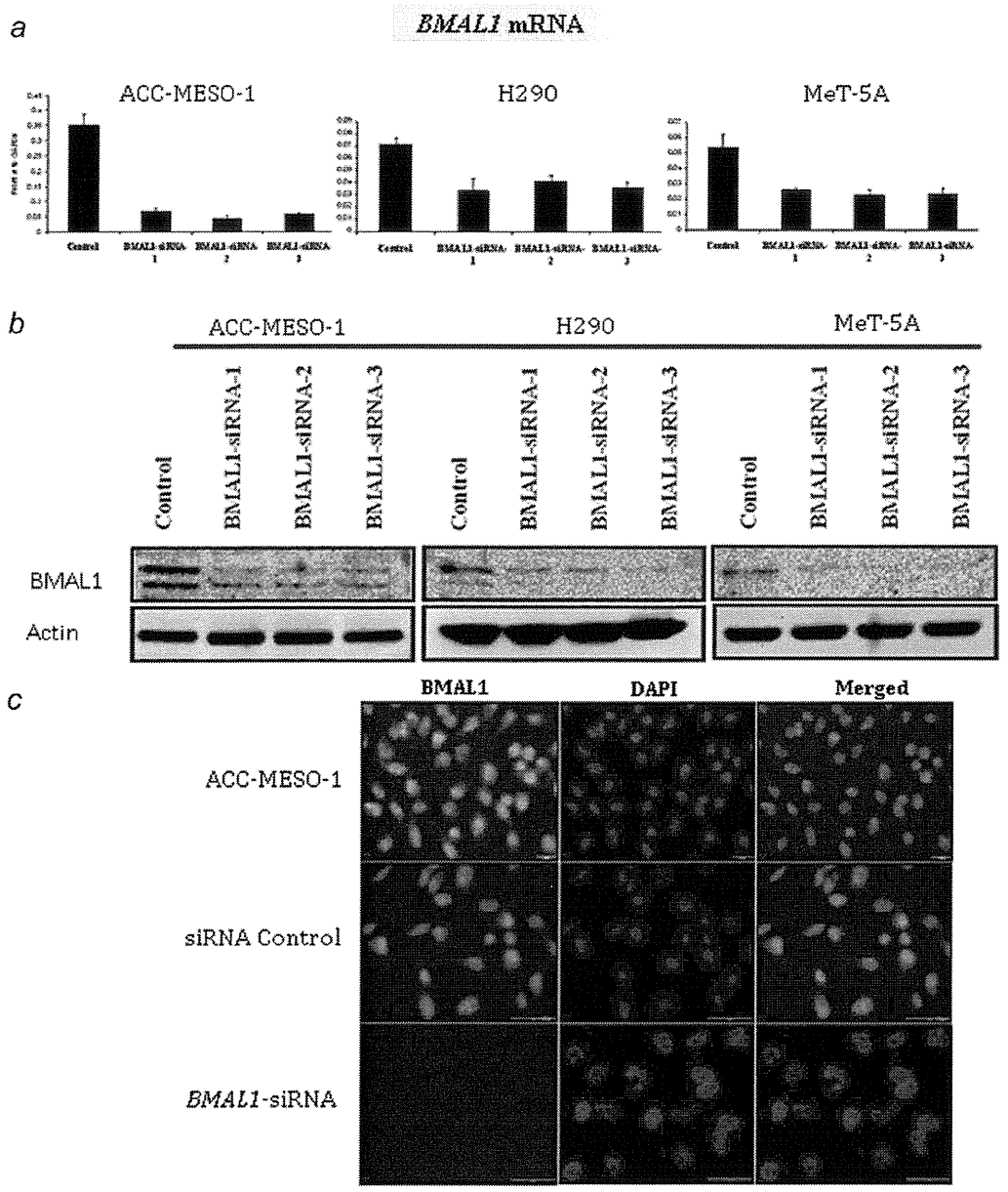

Figure 3. *BMAL1* knockdown in MPM and MeT-5A cells. Confirmation of *BMAL1* knockdown by (*a*) qRT-PCR, (*b*) Western blot analysis and (*c*) immunofluorescence (IF) assay. IF was used to examine BMAL1 levels in the parental, siRNA control or siRNA-BMAL1-treated ACC-MESO-1 cells. All data are averages of three independent experiments done in duplicates. [Color figure can be viewed in the online issue, which is available at wileyonlinelibrary.com.]

6*c*). Importantly, the existence of micronucleation is a highly indicative sign of catastrophic mitosis. To examine the possibility of mitotic catastrophe as a sequel of *BMAL1* knockdown and to explain its role in *BMAL1*-induced cell death during the cell cycle, ACC-MESO-1 cells transfected with *BMAL1*-siRNA or control oligos synchronized using a double thymidine block (to induce pharmacological block of mitosis in these cells). Interestingly, inhibition of mitosis in ACC-MESO-1 transfected with *BMAL1* siRNA resulted in a marked decrease of polyploidy and subG1 population (Fig. 6*d*), suggesting aberrant mitosis as a cause of cell death after BMAL1 knockdown. To confirm the occurrence of mitotic catastrophe following *BMAL1* knockdown, we performed time lapse microscopic examination for ACC-MESO-1 cells transfected with *BMAL1*-siRNA or control oligos. Examination showed that cells rounding up as they entered mitosis, then attempting to undergo cytokinesis. ACC-MESO-1 cells transfected with control siRNA successfully completed mitosis, but *BMAL1* siRNA-treated cells failed to divide properly and exhibited large cell volume and micronucleation (Fig. 6*e*), indicating mitotic catastrophe as a cell fate following BMAL1 knockdown in those cells.

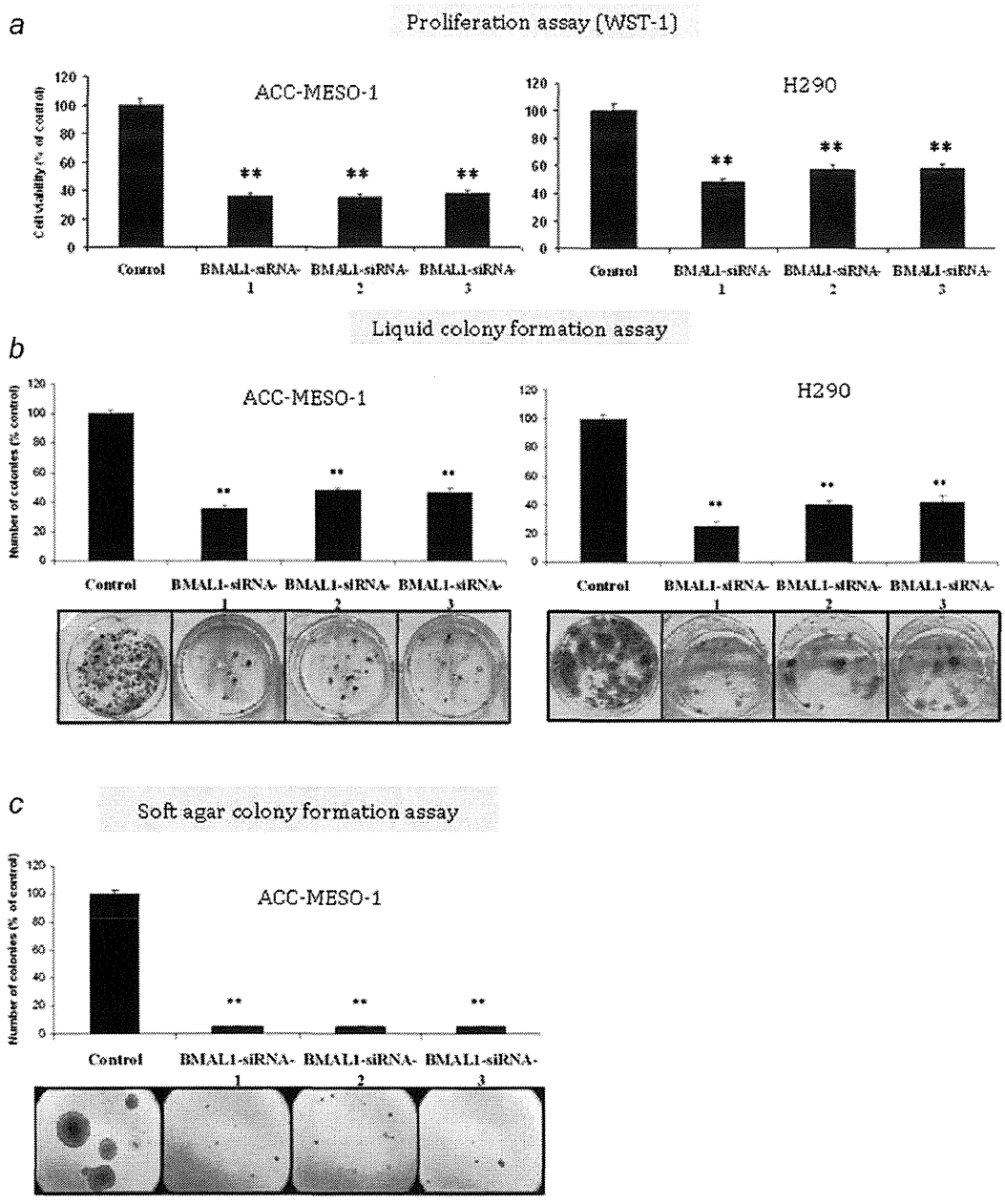

Figure 4. *BMAL1* knockdown inhibits proliferation and suppresses clonal growth of MPM cells in anchorage-dependent and -independent conditions. (*a*) WST-1 proliferation. (*b*) Liquid colony formation assays for ACC-MESO-1 and H290 cells transfected with BMAL1-siRNA or control oligos. (*c*) Soft agar colony formation assay for ACC-MESO-1 cells transfected with BMAL1-siRNA or control oligos. Results are from three independent experiments and shown as mean ± SD. In liquid colony and soft agar assay colony, numbers of cells transfected with control oligos are set as 100%. ** indicate $p < 0.01$ (Mann–Whitney *U* test). All data are averages of three independent experiments done in duplicates. [Color figure can be viewed in the online issue, which is available at wileyonlinelibrary.com.]

RNAi-mediated knockdown of *BMAL1* results in expression alterations of the cell cycle regulators in ACC-MESO-1 cells

Recent data suggest that there is a strong relationship between the circadian clock system and regulation of the cell cycle.[21,22] In particular, *BMAL1* is considered a key regulator of cancer cell proliferation through coordinating the activity of cell cycle proteins including $p21^{WAF1/CIP1}$ and cyclin B. Specifically, some data suggest that the circadian clock controls mitotic process through Wee1, known to be clock target gating the G2/M transition.[10,21,23] Therefore, we investigated the link between *BMAL1* knockdown and the status of the cell cycle proteins. Notably, ACC-MESO-1 cells after *BMAL1* knockdown showed profound alterations in cell cycle

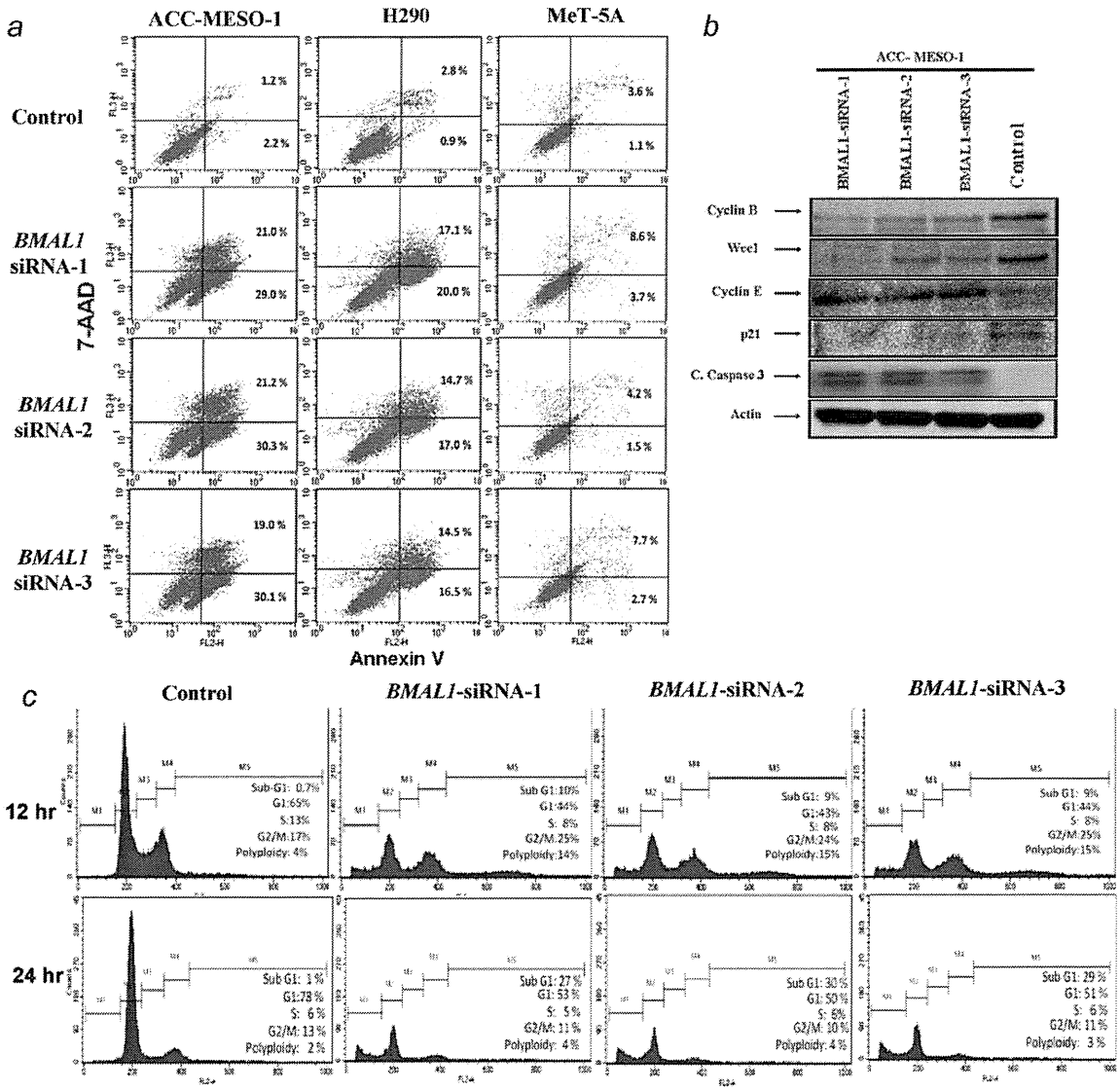

Figure 5. *BMAL1* knockdown induces apoptosis and cell cycle disruption (*a*) FACS analysis of cells costained with anti-annexin V and 7-AAD. High Annexin V and low 7-AAD cells are undergoing apoptosis while cells with low Annexin and high 7-AAD are undergoing necrosis. (*b*) Immunoblot showing effects of *BMAL1* knockdown on its targets in ACC-MESO-1 cells. (*c*) Cell cycle analysis of ACC-MESO-1 cells transfected with *BMAL1*-siRNA or control oligos. Forty-eight-hour post-transfection cells underwent serum starvation for 12 hr (upper panel) and for 24 hr (lower panel) then were harvested with both adherent and floating cells were combined and prepared for cell cycle analysis by flow cytometry, as described in "Material and Methods" Section. Results are the average of two independent experiments. [Color figure can be viewed in the online issue, which is available at wileyonlinelibrary.com.]

regulators, including significant decrease of Wee1, $p21^{WAF1/CIP1}$, cyclin B proteins and accumulation of cyclin E protein (Fig. 5*b*).

Discussion

In this report, we show that most MPM cell lines and a subset of surgically annotated MPM specimens expressed higher levels of *BMAL1* than MeT-5A and normal parietal pleural specimens, respectively. Silencing of *BMAL1* resulted in suppression of MPM cell growth and induction of apoptosis in these cells but limited effect was observed in MeT-5A. *BMAL1* depletion from ACC-MESO-1 cells, which expressed the highest level of *BMAL1*, led to cell cycle disruption with a substantial increase in apoptotic and polyploidy cell population as well as decreased levels of Wee1, cyclin B and $p21^{WAF1/CIP1}$ expression and upregulation of cyclin E. *BMAL1* knockdown in ACC-MESO-1 cells induced mitotic catastrophe denoted by marked disruption of cell cycle regulator proteins and drastic morphological changes including micronucleation, multiple nuclei and increased cellular volume of ACC-MESO-1 cells.

By immunohistochemical analysis, we demonstrated that *BMAL1* is constitutively expressed in a subset of clinical

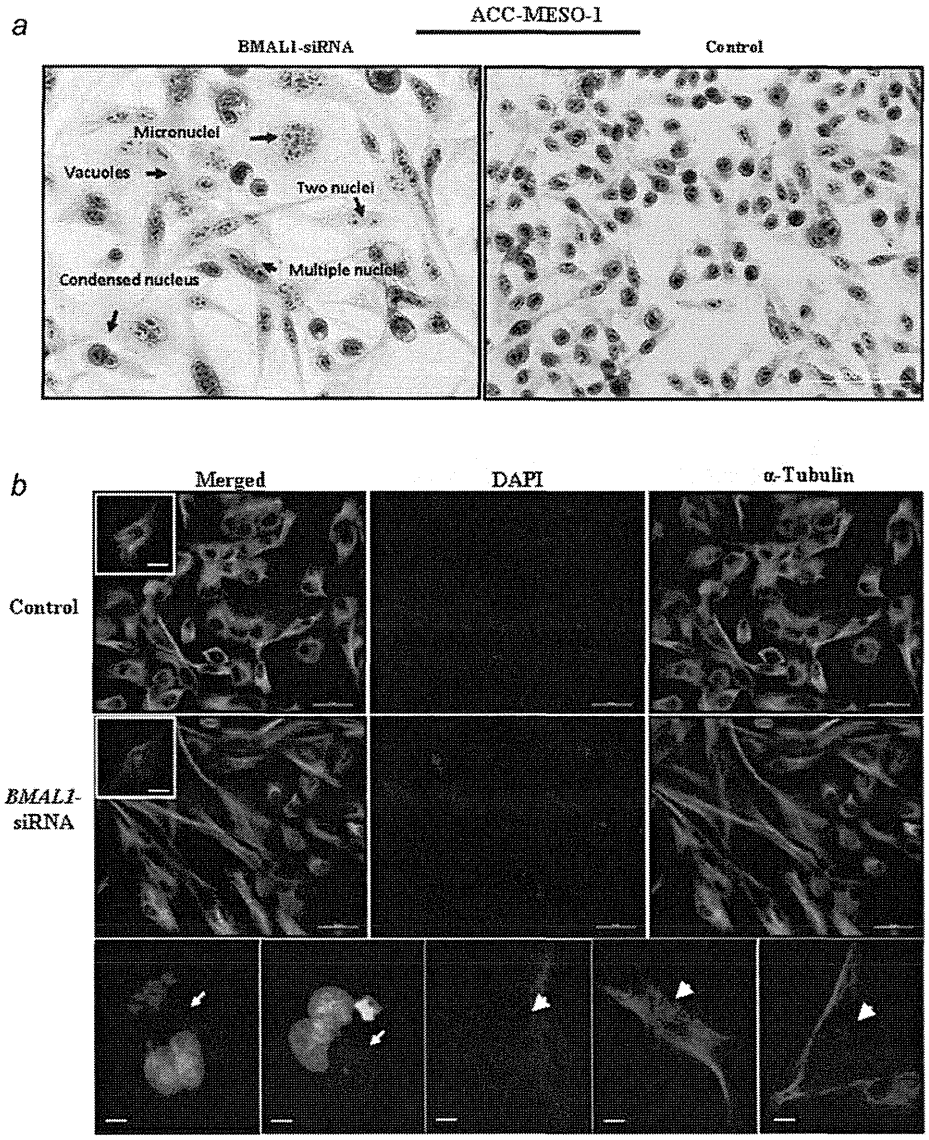

Figure 6. *BMAL1* knockdown induces dramatic morphological alterations in ACC-MESO-1 cells. (*a*) H–E stain showing the nuclear morphological changes identified in ACC-MESO-1 cells after ablation of *BMAL1*. (*b*) IF of α-tubulin and DAPI stains. The upper panels represent ACC-MESO-1 cells treated with siRNA control. The lower panels represent the most frequent morphological changes (arrow indicates micronucleation and arrow head indicates multiple nuclei) in single ACC-MESO-1 cell after *BMAL1* depletion. The middle panels represent ACC-MESO-1 cells treated with *BMAL1* siRNA. (*c*) Quantification of the binuclear, multinuclear and micronuclear phenotypes in ACC-MESO-1 cells after BMAL1 knockdown. (*d*) Cell cycle profiling of ACC-MESO-1 cells showing marked decrease of *BMAL1*-induced cell death and polyploidy formation following mitosis block. ACC-MESO-1 cells transfected with *BMAL1* siRNA or control oligos with double-thymidine (black arrows) and without thymidine treatment (arrow heads) were harvested for analyses of DNA content by flow cytometry. Synchronized cells at late G1/early S by double-thymidine escaped from *BMAL1* knockdown-induced cell death with marked reduction in subG1 and polyploidy formation. (*e*) Time lapse microscopic examination showing the aberrant mitosis in ACC-MESO-1 cells transfected with *BMAL1* siRNA (white arrow head) and intact mitosis in cells transfected with control oligos (white arrow). (*f*) Proposed molecular mechanism of BMAL1 knockdown-induced mitotic catastrophe in ACC-MESO-1 cells. Decreasing cyclin B below a critical level results in mitosis skipping and enhances polyploidy formation. Downregulation of p21WAF1/CIP1 results in accumulation of cyclin E which could lead to increased number of polyploidy cells. Wee1 downregulation could contribute to eventual escape from G2/M arrest, which in turns participates in impairment of mitotic integrity. [Color figure can be viewed in the online issue, which is available at wileyonlinelibrary.com.]

MPM samples. Two out of three Stage IV-MPM patients were positive for BMAL1, whereas three out of 12 Stage III-MPM patients were positive (Table 1). This suggests that BMAL1 expression may be associated with advanced stage-MPM, but the small patients' number makes it difficult to draw a firm conclusion on this possible association (Supporting Information, Fig. S2). It would be of importance to analyze the association between BMAL1 expression and

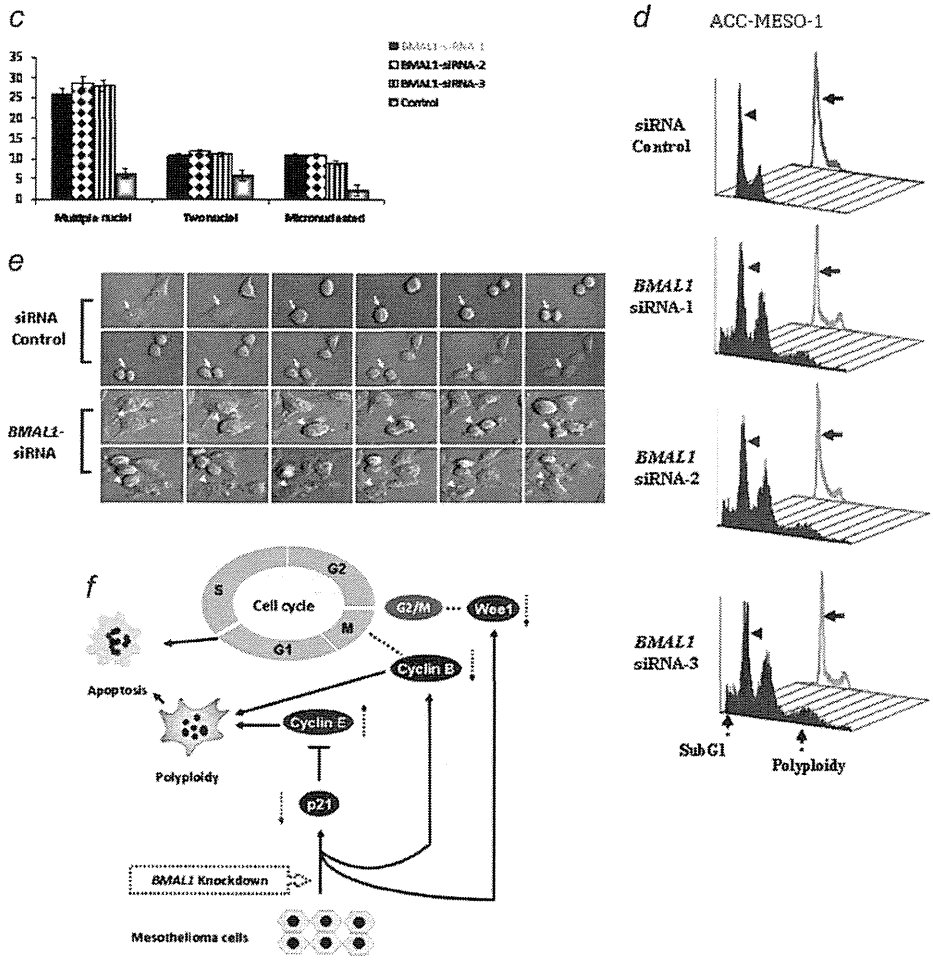

Figure 6. (Continued).

clinicopathological features of MPM using a large cohort. In line with our provisional results, high BMAL1 expression was observed in metastatic breast, colorectal and liver cancers,[12,13] these findings suggest that *BMAL1* has an oncogenic activities in a variety of human cancers.

A prior study reported that clock genes oscillation was found in different tissues including muscle, liver and adipose tissues.[24] *BMAL1* rhythmic expression was observed also in NIH3T3 cell following synchronization by serum shock.[25] Here, we found that the rhythmic expression of *BMAL1* over the 24 hr period was intact and clearly observed in NIH3T3 cells and MeT-5A as well. Intriguingly, ACC-MESO-1 cells showed constant levels of *BMAL1* mRNA. This result is consistent with a recent report[20] showing that *BMAL1* is rhythmically expressed in mouse prostate while serum-shocked synchronized prostate cancer cells showed disrupted circadian rhythmicity of *BMAL1* gene. In line with Roe *et al.*'s[15] results who reported that *BMAL1* was found to be overexpressed concomitantly with downregulation of its negative counterpart in MPM compared to the normal parietal pleural tissue, our findings support the notion that the circadian rhythm pathway could be deregulated in MPM.

We demonstrated that inhibition of *BMAL1* expression using RNAi technique significantly suppressed proliferation, anchorage-dependent and independent clonal growth in MPM cells. To explore how *BMAL1* knockdown induced growth inhibition, we performed apoptosis assays and found that depletion of *BMAL1* expression by siRNA resulted in a significant increase in the fraction of apoptotic and necrotic cells in the MPM cell lines (ACC-MESO-1 and H290) with limited effect in MeT-5A. We also examined the regulatory role of *BMAL1* in MPM cell cycle and its importance in sustained cell proliferation. Interestingly, we found that RNAi-mediated knockdown of *BMAL1* resulted in cell cycle disruption of ACC-MESO-1 cells but not in MeT-5A cells.

Following *BMAL1* transient knockdown, we observed multiple morphological abnormalities consistent with aberrant mitotic process. There was an increase of binucleated cells, which may correspond to the modest increase in the G2/M phase cell population. Furthermore, some other cells

(about 10%) showed micronucleation. Bergman *et al.*[26] reported that the occurrence of cells with double nucleus suggests that these cells undergo cell division without segregating their DNA and could be explained by the increase in cells with 4 *N* DNA content seen with flow cytometry. Importantly, micronucleation is highly indicative of mitotic catastrophe and could be resulted from chromosomal missegregation caused by DNA breaks. It is quite possible that ACC-MESO-1 cells underwent mitotic catastrophe due to impairment of cell cycle regulator proteins, such as, cyclin B, $p21^{WAF1/CIP1}$ and Wee1 (Fig. 6*f*). It is demonstrated that decreasing cyclin B below a critical level results in mitosis skipping and enhances polyploidy formation, which is considered as one of the characteristics of mitotic catastrophe.[27] Polyploidy cells pass an extra round of cell cycle and finally undergo apoptosis.[28] In addition, Wee1 downregulation could contribute to eventual escape from G2/M arrest, which in turns participates in impairment of mitotic integrity. In this study, we observed downregulation of $p21^{WAF1/CIP1}$ and cyclin E upregulation following *BMAL1* knockdown, and the latter could also lead to increased number of polyploidy cells. Other investigators noted that *BMAL1* modulate the transcriptional activity of p53 toward its target p21 and clearly showed that *BMAL1* knockdown caused a decrease in p21 level.[22] Moreover, a previous study reported that overexpression of cyclin E led to impairment of mitosis and polyploidy formation.[29] We believe that accumulation of polyploidy, large multinucleated cells and micronucleation in ACC-MESO-1 after *BMAL1* knockdown were consistent with cell death mechanism involving mitotic catastrophe. It has been shown that mitotic catastrophe could be considered as an important safeguard to prevent the proliferation of polyploidy cells[30] and apoptosis frequently follows mitotic catastrophe.[31] Taken together, these findings show that *BMAL1* plays a critical role in the mitotic process of cancer cells. To our knowledge, this study is the first to shed light on the involvement of *BMAL1* in polyploidy formation, impairment of mitotic events, and also to highlight the role of circadian clock genes in MPM. In conclusion, we provide evidence that BMAL1 plays an important role and it may be a promising therapeutic target for MPM, but careful consideration is needed to avoid the counter effect on tissues dependant on BMAL1 such as muscles and liver.

References

1. Robinson BW, Musk AW, Lake RA. Malignant mesothelioma. *Lancet* 2005;366:397–408.
2. Sekido Y. Molecular biology of malignant mesothelioma. *Environ Health Prev Med* 2008;13: 65–70.
3. Tsao AS, Wistuba I, Roth JA, et al. Malignant pleural mesothelioma. *J Clin Oncol* 2009;27: 2081–90.
4. Taniguchi H, Fernandez AF, Setien F, et al. Epigenetic inactivation of the circadian clock gene *BMAL1* in hematologic malignancies. *Cancer Res* 2009;69:8447–54.
5. Balsalobre A, Damiola F, Schibler U. A serum shock induces circadian gene expression in mammalian tissue culture cells. *Cell* 1998;93: 929–37.
6. Straif K, Baan R, Grosse Y, et al. Carcinogenicity of shift-work, painting, and fire-fighting. *Lancet Oncol* 2007;8:1065–6.
7. Canaple L, Kakizawa T, Laudet V. The days and nights of cancer cells. *Cancer Res* 2003;63: 7545–52.
8. Bunger MK, Wilsbacher LD, Moran SM, et al. Mop3 is an essential component of the master circadian pacemaker in mammals. *Cell* 2000;103: 1009–17.
9. Gauger MA, Sancar A. Cryptochrome, circadian cycle, cell cycle checkpoints, and cancer. *Cancer Res* 2005;65:6828–34.
10. Matsuo T, Yamaguchi S, Mitsui S, et al. Control mechanism of the circadian clock for timing of cell division in vivo. *Science* 2003;302: 255–9.
11. Fu L, Lee CC. The circadian clock: pacemaker and tumour suppressor. *Nat Rev Cancer* 2003;3: 350–61.
12. Oshima T, Takenoshita S, Akaike M, et al. Expression of circadian genes correlates with liver metastasis and outcomes in colorectal cancer. *Oncol Rep* 2011;25:1439–46.
13. Kuo SJ, Chen ST, Yeh KT, et al. Disturbance of circadian gene expression in breast cancer. *Virchows Arch* 2009;454:467–74.
14. Koyanagi S, Kuramoto Y, Nakagawa H, et al. A molecular mechanism regulating circadian expression of vascular endothelial growth factor in tumor cells. *Cancer Res* 2003;63:7277–83.
15. Roe OD, Anderssen E, Helge E, et al. Genome-wide profile of pleural mesothelioma versus parietal and visceral pleura: the emerging gene portrait of the mesothelioma phenotype. *PLoS One* 2009;4:e6554.
16. Usami N, Fukui T, Kondo M, et al. Establishment and characterization of four malignant pleural mesothelioma cell lines from Japanese patients. *Cancer Sci* 2006;97:387–94.
17. Takeyama Y, Sato M, Horio M, et al. Knockdown of *ZEB1*, a master epithelial-to-mesenchymal transition (EMT) gene, suppresses anchorage-independent cell growth of lung cancer cells. *Cancer Lett* 2010;296:216–24.
18. Husain AN, Colby TV, Ordonez NG, et al. Guidelines for pathologic diagnosis of malignant mesothelioma: a consensus statement from the International Mesothelioma Interest Group. *Arch Pathol Lab Med* 2009;133:1317–31.
19. Sato M, Vaughan MB, Girard L, et al. Multiple oncogenic changes (K-RAS(V12), p53 knockdown, mutant EGFRs, p16 bypass, telomerase) are not sufficient to confer a full malignant phenotype on human bronchial epithelial cells. *Cancer Res* 2006;66:2116–28.
20. Cao Q, Gery S, Dashti A, et al. A role for the clock gene per1 in prostate cancer. *Cancer Res* 2009;69:7619–25.
21. Grechez-Cassiau A, Rayet B, Guillaumond F, et al. The circadian clock component BMAL1 is a critical regulator of p21WAF1/CIP1 expression and hepatocyte proliferation. *J Biol Chem* 2008; 283:4535–42.
22. Mullenders J, Fabius AW, Madiredjo M, et al. A large scale shRNA barcode screen identifies the circadian clock component ARNTL as putative regulator of the p53 tumor suppressor pathway. *PLoS One* 2009;4:e4798.
23. Wood PA, Du-Quiton J, You S, et al. Circadian clock coordinates cancer cell cycle progression, thymidylate synthase, and 5-fluorouracil therapeutic index. *Mol Cancer Ther* 2006;5: 2023–33.
24. Yang X, Downes M, Yu RT, et al. Nuclear receptor expression links the circadian clock to metabolism. *Cell* 2006;126:801–10.
25. Yagita K, Tamanini F, van Der Horst GT, et al. Molecular mechanisms of the biological clock in cultured fibroblasts. *Science* 2001;292: 278–81.
26. Bergman LM, Birts CN, Darley M, et al. CtBPs promote cell survival through the maintenance of mitotic fidelity. *Mol Cell Biol* 2009;29:4539–51.
27. Galimberti F, Thompson SL, Ravi S, et al. Anaphase catastrophe is a target for cancer therapy. *Clin Cancer Res* 2011;17:1218–22.
28. Li S, Szymborski A, Miron MJ, et al. The adenovirus E4orf4 protein induces growth arrest and mitotic catastrophe in H1299 human lung carcinoma cells. *Oncogene* 2009;28:390–400.
29. Keck JM, Summers MK, Tedesco D, et al. Cyclin E overexpression impairs progression through mitosis by inhibiting APC(Cdh1). *J Cell Biol* 2007;178:371–85.
30. Marrazzo E, Marchini S, Tavecchio M, et al. The expression of the DeltaNp73beta isoform of p73 leads to tetraploidy. *Eur J Cancer* 2009;45: 443–53.
31. Rivera A, Mavila A, Bayless KJ, et al. Cyclin A1 is a p53-induced gene that mediates apoptosis, G2/M arrest, and mitotic catastrophe in renal, ovarian, and lung carcinoma cells. *Cell Mol Life Sci* 2006;63:1425–39.

Published OnlineFirst August 19, 2011; DOI:10.1158/0008-5472.CAN-11-1020

Cancer Research

miR-375 Is Activated by ASH1 and Inhibits YAP1 in a Lineage-Dependent Manner in Lung Cancer

Eri Nishikawa, Hirotaka Osada, Yasumasa Okazaki, et al.

Cancer Res 2011;71:6165-6173. Published OnlineFirst August 19, 2011.

Published OnlineFirst August 19, 2011; DOI:10.1158/0008-5472.CAN-11-1020

Molecular and Cellular Pathobiology

Cancer Research

miR-375 Is Activated by ASH1 and Inhibits YAP1 in a Lineage-Dependent Manner in Lung Cancer

Eri Nishikawa[1], Hirotaka Osada[2,4], Yasumasa Okazaki[3], Chinatsu Arima[1], Shuta Tomida[1], Yoshio Tatematsu[4], Ayumu Taguchi[1], Yukako Shimada[1], Kiyoshi Yanagisawa[6], Yasushi Yatabe[5], Shinya Toyokuni[3], Yoshitaka Sekido[2,4], and Takashi Takahashi[1]

Abstract

Lung cancers with neuroendocrine (NE) features are often very aggressive but the underlying molecular mechanisms remain elusive. The transcription factor ASH1/ASCL1 is a master regulator of pulmonary NE cell development that is involved in the pathogenesis of lung cancers with NE features (NE-lung cancers). Here we report the definition of the microRNA *miR-375* as a key downstream effector of ASH1 function in NE-lung cancer cells. *miR-375* was markedly induced by ASH1 in lung cancer cells where it was sufficient to induce NE differentiation. *miR-375* upregulation was a prerequisite for ASH1-mediated induction of NE features. The transcriptional coactivator YAP1 was determined to be a direct target of *miR-375*. YAP1 showed a negative correlation with *miR-375* in a panel of lung cancer cell lines and growth inhibitory activities in NE-lung cancer cells. Our results elucidate an ASH1 effector axis in NE-lung cancers that is functionally pivotal in controlling NE features and the alleviation from YAP1-mediated growth inhibition. *Cancer Res; 71(19); 6165–73. ©2011 AACR.*

Introduction

Lung cancer has long been the leading cause of cancer-related death in economically developed countries, and a better understanding of the molecular pathogenesis of this fatal disease is greatly anticipated for preventive and/or therapeutic breakthroughs (1). Accumulated evidence strongly suggests that alterations of microRNA (miRNA) expressions are involved in the development of human cancers (2–5). Our previous studies identified *let-7* as a miRNA family with growth inhibitory activities, which were also found to be frequently downregulated in lung cancers in association with poor prognosis (6). In marked contrast to the tumor suppressor-like *let-7* miRNA family, the *miR-17-92* miRNA cluster plays roles as oncogene-type miRNAs in the development of lung cancers (7, 8).

Lung cancer is classified into 2 major classes, small cell lung cancer (SCLC) and non-SCLC (NSCLC), of which SCLC characteristically exhibits neuroendocrine (NE) features and an aggressive clinical course. In addition, a small proportion of NSCLCs such as large cell NE carcinoma also share such characteristics. Therefore, it is conceivable that elucidation of the underlying mechanisms involved in the acquisition of those characteristics in lung cancers with NE features may provide important clues for a better understanding of carcinogenic processes. Along this line, we previously reported that A549 lung adenocarcinoma cells exhibited NE properties when introduced with achaete-scute homologue 1 (ASH1/ASCL1), a proneural basic helix-loop-helix (bHLH) transcription factor (9), whereas ASH1 knockdown elicited prominent apoptosis in SCLC lung cancer cell lines (10). We also found that ASH1 mediates lineage-survival signal in SCLC at least in part through its transcriptional repressor activity toward putative tumor suppressor including *DKK1* and *E-cadherin* (9). However, to date, virtually nothing is known about the possible involvement of miRNAs downstream of this dual function transcription factor, which is crucially involved in the biology of SCLC.

In this study, we investigated whether miRNAs are also governed by ASH1 and have roles downstream of ASH1 in the development of lung cancers with NE features. Consequently, *miR-375* was identified as a miRNA directly and highly transactivated by ASH1. The involvement of *miR-375* in acquisition of NE phenotypes and growth regulation in lung cancers with NE features is also discussed.

Authors' Affiliations: [1]Division of Molecular Carcinogenesis, Center for Neurological Diseases and Cancer, [2]Department of Cancer Genetics, Program in Function Construction Medicine, and [3]Department of Pathology and Biological Responses, Nagoya University Graduate School of Medicine; [4]Division of Molecular Oncology, Aichi Cancer Center Research Institute; [5]Department of Pathology and Molecular Diagnostics, Aichi Cancer Center Hospital; and [6]Institute for Advanced Research, Nagoya University, Nagoya, Japan

Note: Supplementary data for this article are available at Cancer Research Online (http://cancerres.aacrjournals.org/).

E. Nishikawa and H. Osada contributed equally to this work.

Corresponding Author: Takashi Takahashi, Division of Molecular Carcinogenesis, Center for Neurological Diseases and Cancer, Nagoya University Graduate School of Medicine, Nagoya, Japan. E-mail: tak@med.nagoya-u.ac.jp or Hirotaka Osada, Aichi Cancer Center Research Institute, Nagoya, Japan. E-mail: hosada@aichi-cc.jp

doi: 10.1158/0008-5472.CAN-11-1020

Published OnlineFirst August 19, 2011; DOI:10.1158/0008-5472.CAN-11-1020

Materials and Methods

Cells and expression constructs

An A549 lung adenocarcinoma cell line without NE differentiation and a typical SCLC cell line, ACC-LC-172, as well as A549 cells stably transduced with ASH1-expressing (A549-ASH1) or empty (A549-VC) lentiviruses (9) were maintained in RPMI-1640 with 5% FBS. ASH1-expressing lentiviral and plasmid vectors were constructed with CSII-CMV-MCS-IRES2-Blasticidin and pcDNA3 (Invitrogen), respectively, as previously described (9). Yes-associated protein 1 (YAP1) cDNA was purchased from OriGene and inserted into CSII-EF-MCS-IRES2-Venus. The lentivirus vectors were kindly provided by Dr. H. Miyoshi (RIKEN BioResource Center). Venus (improved YFP) was provided by Dr. A. Miyawaki (RIKEN Brain Science Institute).

Reporter assay

A 1,028-bp-long putative promoter fragment spanning from 992 bp upstream of the *pre-miR-375* sequence to 3 bp upstream of the mature *miR-375* sequence was amplified from human genomic DNA and cloned into a pGL4.10 basic reporter (pGL4-375P in Fig. 1B). pGL4-Δ1, -Δ2, and -Δ3 truncated reporter plasmids were constructed by reamplification of the pGL4-375P plasmid, with each containing 103, 324, and 681 bp regions 5′ to the *pre-miR-375* sequence (Fig. 1B; Supplementary Fig. S1B). E-box deletion mutant reporters were also constructed by PCR-mediated *in vitro* mutagenesis of pGL4-Δ3. Each of these *miR-375* promoter reporters was transfected into A549 cells using Lipofectamine 2000 (Invitrogen) together with an ASH1 expression vector, pcDNA3-ASH1, or control empty vector, pcDNA3, with the renilla luciferase reporter pRL-TK used as an internal control.

microRNA microarray and gene expression microarray analysis

Microarray analysis was conducted to examine miRNA expression profiles using a Human miRNA Microarray, precommercial version 6.0 (Agilent) with 470 miRNA probes, according to the manufacturer's instructions. A549 cells were infected with an ASH1-expressing or empty lentivirus and harvested 4 days later. miRNA microarray data were $\log_2$ transformed and normalized to the 75th percentile. Microarray analysis by a Whole Human Genome 4 × 44K Microarray G4112F (Agilent) was also conducted to examine changes in expression of potential target genes of *miR-375* by transfection of Pre-miR-375 or Pre-miR-NC#2 (Ambion) in A549 cells, which were then harvested at 12, 24, 48, and 96 hours after transfection. RNA samples were prepared by using an RNeasy kit (Qiagen) as previously described. All the microarray data used for this study are available at Gene Expression Omnibus accession numbers GSE31565 and GSE31566).

Quantitative reverse transcriptase PCR

Quantitative reverse transcriptase PCR (RT-PCR) analysis was carried out by using primers for chromogranin A (CHGA), chromogranin B (CHGB), secretogranin II (SCG2), secretogranin III (SCG3), ASH1, YAP1, and β-actin (Supplementary Table S1), along with Power SYBR Green PCR Master Mix (Applied Biosystems), and an ABI Prism7500 (Applied Biosystems), as previously described. Expression levels were calculated by using the standard curve method and normalized with the expression of β-actin. The expression of *miR-375* was determined by quantitative RT-PCR analysis by using a TaqMan MicroRNA Assay and TaqMan MicroRNA RT Kit (Applied Biosystems). The expression level of *miR-375* was normalized with that of the noncoding RNA *RNU48*.

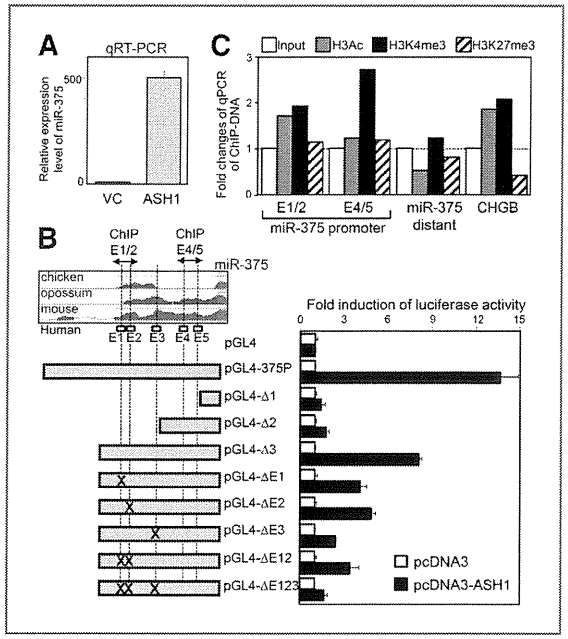

Figure 1. Characterization of the putative *miR-375* promoter. A, induction of *miR-375* by ASH1. The expression of miRNAs in ASH1-infected A549 was determined by microRNA quantitative RT-PCR analyses. B, reporter assay. Putative *miR-375* promoter reporters were transfected into A549 cells together with an ASH1 expression vector, pcDNA3-ASH1, or a control empty vector, pcDNA3. The reporter plasmids pGL4-Δ1, -Δ2, and -Δ3 contain promoter fragments that are 103, 324, and 681 bp upstream from the start site of *pre-miR-375*, as indicated in Supplementary Figure S1B. Deletions of conserved E-boxes (E1–E5) are indicated by "X" marks. C, quantitative ChIP assay. ChIP assays with antibodies against various histone H3 modifications were carried out by A549-ASH1 and ASH1-VC cells. PCR products of the ChIP E1/2 and ChIP E4/5 regions, indicated by arrows in (B), were measured. The ratios of A549-ASH1 cells against A549-VC cells are shown as fold changes. PCR findings for both ChIP E1/2 and ChIP E4/5 showed increases in activation of histone modifications (H3Ac and H3K4me3) in the *miR-375* promoter, whereas distant primers did not show any activating histone modifications.

Quantitative ChIP assay

ChIP assays were carried out as described previously, using ChIP E1/2 and ChIP E4/5 primers, which were designed for amplification of genomic fragments containing E1 and E2 E-boxes and E4 and E5 E-boxes, respectively (Fig. 1B). ChIP analysis using "distant" primers for amplification of a genomic

Published OnlineFirst August 19, 2011; DOI:10.1158/0008-5472.CAN-11-1020

region approximately 5.3 kb downstream of *pre-miR-375* (Supplementary Fig. S1) as well as CHGB primers were used as negative and positive controls, respectively. The primer sequences are shown in Supplementary Table S1. The amounts of chromatin-immunoprecipitated genomic DNA were measured by the ΔΔCt method to compare various ChIP primers and β-actin primers and the results of quantification were obtained as fold changes of A549-ASH1 against A549-VC. Antibodies against acetylated histone H3 (H3Ac), trimethylated H3 lysine 4 (H3K4me3), and trimethylated H3 lysine 27 (H3K27me3) were purchased from Upstate.

In situ hybridization

We employed a Fluorescein isothiocyanate–labeled locked nucleic acid (LNA) probe for *mmu-miR-375* and a scrambled sequence (Exiqon). Probes were diluted to 40 nmol/L in hybridization buffer (Ambion). *In situ* hybridization was conducted according to the manufacturer's protocol, as previously described (11). In brief, after deparaffinization, neutral formalin-fixed specimens on slides were incubated in proteinase K solution (20 μg/mL) at 37°C. After fixing the specimens with 4% paraformaldehyde, endogenous peroxidase activities were quenched in methanol containing H_2O_2 [0.3% (v/v)], then the probes were hybridized overnight at 37°C. After washing with SSC with 50% formamide, a CSA II biotin-free catalyzed signal amplification system (Dako) was used to visualize miRNA expression as brown precipitates. Nuclear staining was done with hematoxylin.

Immunohistochemical analysis

Slides were subjected to an antigen retrieval procedure by using Immunosaver (Nisshin EM) and then endogenous peroxidase activities were quenched. Next, the slides were incubated with rabbit polyclonal antisynaptophysin antibody (Dako) followed by goat anti-rabbit immunoglobulins/horseradish peroxidase (Dako), and then visualized with liquid 3,3′-diaminobenzidine (Dako). Nuclear counterstaining was done with hematoxylin.

Transfection of Pre-miR-375 and LNA

Both Pre-miR-375 and Pre-miR-NC#2 were purchased from Ambion. Antisense and scramble oligonucleotides against mature *miR-375* were synthesized by using LNAs (Greiner). Each of oligonucleotides was introduced into A549 cells at 10 to 15 nmol/L, using 2.5 μL/mL of Lipofectamine RNAiMax (Invitrogen) according to the instructions of supplier.

Results

This study was initiated to investigate the potential involvement of miRNAs downstream of ASH1 in acquisition of characteristics of lung cancers with NE features. To this end, we first carried out genome-wide expression profiling of miRNAs to search for those significantly affected by ASH1 transduction in a lung cancer cell line without NE features. As a result, we identified 12 upregulated (>5-fold) and 8 downregulated (>5-fold) miRNAs in ASH1-transduced A549 cells (Table 1), of which *miR-375* was found to be the most highly

Table 1. Up- and downregulated miRNAs in ASH1-transduced A549 cells

miRNA	A549-ASH1[a]	A549-VC[a]	Fold change
Upregulated miRNAs (>5-fold)			
hsa-miR-375	62.806	0.038	1,659.802
hsa-miR-193a	8.071	0.726	11.120
hsa-miR-489	0.332	0.030	11.105
hsa-miR-10a	13.254	1.333	9.940
hsa-miR-196b	0.231	0.030	7.731
hsa-miR-181a	4.906	0.683	7.188
hsa-miR-181a*	0.185	0.026	7.108
hsa-miR-95	0.178	0.026	6.830
hsa-miR-326	0.353	0.052	6.785
hsa-miR-9*	2.559	0.397	6.441
hsa-miR-628	0.149	0.026	5.720
hsa-miR-181b	8.344	1.512	5.517
Downregulated miRNAs (>5-fold)			
hsa-miR-200b	0.018	1.008	0.018
hsa-miR-30a-3p	0.018	0.608	0.029
hsa-miR-137	0.018	0.467	0.038
hsa-miR-200a	0.018	0.455	0.039
hsa-miR-30a-5p	1.092	13.985	0.078
hsa-miR-149	0.116	1.363	0.085
hsa-miR-618	0.041	0.255	0.161
hsa-miR-422b	0.463	2.485	0.186

[a]Normalized signal intensity.

Published OnlineFirst August 19, 2011; DOI:10.1158/0008-5472.CAN-11-1020

upregulated, which was also verified by quantitative RT-PCR, using an *miR-375*–specific TaqMan probe (Fig. 1A). An ASH1 lentivirus was also transduced into 4 other NSCLC cell lines, 3 of which showed marked *miR-375* induction (Supplementary Fig. S2A). A survey of the genomic region harboring *miR-375* indicated that this miRNA resides in an intergenic region between the *CCDC108* and *CRVBA2* genes at chromosome 2q35 (Supplementary Fig. S1A), whereas a region approximately 1 kb in length was found to be evolutionally highly conserved (shown in red). Of the 5 conserved E-boxes, 4 were CACCTG whereas the other (E2) was CATCTG. To verify the promoter activity and responsiveness to ASH1, luciferase reporter constructs of the putative *miR-375* promoter and its various mutants were cotransfected with an ASH1 expression vector, pcDNA3-ASH1, or an empty vector into A549 cells. The pGL4-375P showed marked transactivation by ASH1 (Fig. 1B). pGL4-Δ3 containing 3 E-boxes (E1 to E3) showed robust responsiveness to ASH1, whereas pGL4-Δ2 with a further deletion failed to respond. Reporters, each of which contained a single E-box deletion mutation (pGL4-ΔE1, -ΔE2, and -ΔE3), showed moderate reductions in ASH1 responsiveness, whereas pGL4-ΔE123, carrying a deletion of all 3 E-boxes (E1 to E3), lost responsiveness to a level similar to that of pGL4-Δ2, indicating their crucial involvement in ASH1 responsiveness. To further confirm the promoter activity of this region, ChIP assays with antibodies against various histone H3 modifications were carried out by A549 cells infected with either ASH1-carrying or empty viruses (Fig. 1C). Consequently, specific induction of activating histone modifications (H3Ac and H3K4me3) in the genomic regions encompassing these 3 E-boxes were clearly shown in ASH1-expressing A549 cells. In addition, a ChIP assay with an anti-myc-tag antibody against the myc-tagged ASH1 protein indicated a direct interaction of ASH1 with the E1/2 region (Supplementary Fig. S3).

The association between ASH1 and *miR-375* expression was then analyzed in fetal mouse lung (Fig. 2A). Although neuroepithelial bodies (NEB), known to consist of ASH1-expressing pulmonary NE cells and epithelial progenitor cells (12), showed positive immunohistochemical staining for the NE marker synaptophysin, *in situ* hybridization showed coexpression of *miR-375*, showing that ASH1–*miR-375* signal is associated with NE differentiation. We also noted that *miR-375* was also detectable in pancreatic islet cells despite a lack of ASH1 expression, suggesting other mechanisms for its induction in the pancreas (Supplementary Fig. S4A). We observed histologic type-dependent expression of *miR-375* in the present lung cancer cell lines (Fig. 2B). A high level of expression was specifically detected in SCLC cell lines, which generally express ASH1 and have NE features (Fig. 2B). A moderate expression of *miR-375* was observed in large cell carcinoma cell lines, whereas *miR-375* was detected in a few exceptional adenocarcinoma cell lines, but in none of the squamous carcinoma cell lines. In addition, a positive correlation was seen between *miR-375* and ASH1 expression in the lung cancer cell lines (data not shown). Our *in situ* hybridization analysis revealed a positive signal for *miR-375* in the ACC-LC-172 SCLC cell line, whereas A549 did not show any signals (Supplementary Fig. S4B and C).

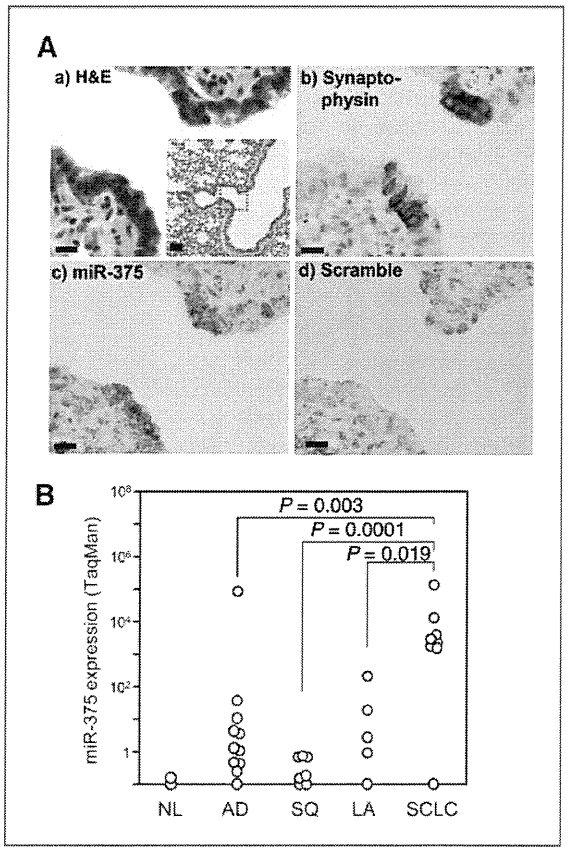

Figure 2. *miR-375* expression in normal lung and lung cancers. A, *in vivo* expression of *miR-375* in NEBs from fetal mouse lung tissue. a, hematoxylin and eosin (H&E) staining of normal fetal lung tissue containing 2 NEBs. The area with 2 NEBs enclosed by a red line is shown magnified in (a–d). b, IHC staining with antibody against the NE marker, synaptophysin. c and d, *in situ* hybridization with an *miR-375* antisense oligo (c) and scramble control oligo (d). Combinational analyses with IHC and *in situ* hybridization results showed restricted expressions of synaptophysin, and *miR-375* in NEBs. a (inset), magnification, 4×; black bar, 50 μm. a–d, magnification, 40×; black bar, 10 μm. B, expression levels of *miR-375* in lung cancer cell lines. NL, normal lung; AD, adenocarcinoma; SQ, squamous cell carcinoma; LA, large cell carcinoma. The SCLC cell lines showed significantly elevated expression of *miR-375*, whereas only moderate expression was observed in most of the LA cells. Only a few AD cell lines showed the expression of *miR-375*. Overexpression of *miR-375* in SCLC was statistically significant as compared with that expression in lung cancers of other histologic types.

We next investigated the functional significance of ASH1-inducible *miR-375* in terms of biological phenotypes of ASH1-positive lung cancer cells. To this end, we conducted genome-wide expression profiling analysis of *miR-375*–transfected A549 cells (Fig. 3A). Two hundred fifty-three genes exhibited greater than 2-fold changes in their expression levels between 12 and 96 hours after transfection. Interestingly, we noted that multiple NE-related genes were gradually induced at 48 and 96 hours after *miR-375* introduction, which was also confirmed by quantitative RT-PCR analysis results (Fig. 3B). As this finding strongly suggests that *miR-375* alone is capable of inducing NE

Published OnlineFirst August 19, 2011; DOI:10.1158/0008-5472.CAN-11-1020

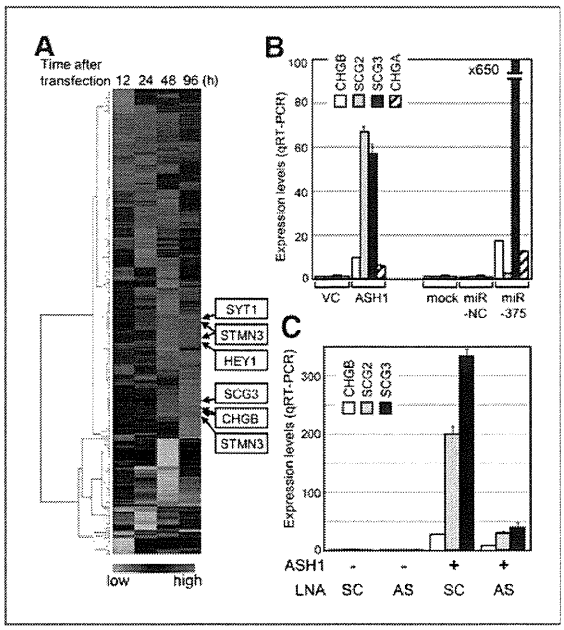

Figure 3. Gene expression profiling and NE induction after Pre-miR-375 transfection. A, the expression ratio of each gene of Pre-miR-375–transfected cells to those of Pre-miR-NC#2–transfected cells was analyzed by clustering. Time course (12–96 hours) of gene expression profiles after Pre-miR-375 transfection. Two hundred fifty-three genes showed greater than 2-fold changes in expression level. Genes related to NE features were indicated. SYT1, synaptotagmin I; STMN3, stathmin-like 3; HEY1, hairy/enhancer-of-split related with YRPW motif 1; SCG3, secretogranin III. B, induction of NE markers by *miR-375*. The expressions of NE markers were measured by quantitative RT-PCR. A549 cells transfected with Pre-miR-375 showed strong induction of NE markers as well as A549-ASH1 cells. C, inhibition of NE markers by *miR-375* antisense LNA. First, infection was performed with an ASH1-expressing or empty lentivirus, then *miR-375* antisense or scramble LNA was transfected into A549 cells. Strong inductions of NE markers by ASH1 were significantly inhibited by *miR-375* antisense LNA. AS, antisense; SC, scramble.

markers in the absence of ASH1, we then investigated whether *miR-375* is required for NE marker induction by ASH1. A549 cells were first infected with an ASH1-expressing lentivirus and subsequently transfected with *miR-375* antisense or scramble LNAs, which resulted in marked inhibition of ASH1-mediated induction of various NE markers in the presence of *miR-375* antisense, but not negative control, *miR-375* scramble (Fig. 3C). These findings clearly showed that ASH1-inducible *miR-375* is required for NE marker induction by ASH1 in lung cancer cells. To verify the specificity of NE marker induction by *miR-375*, we also transfected unrelated miRNAs into A549 cells. As shown in Supplementary Fig. S2B, various unrelated miRNAs scarcely induced CHGB expression, suggesting the specificity of *miR-375*–mediated NE marker induction. In addition, *miR-375* was transfected into 2 other NSCLC cell lines and 2 immortalized normal lung epithelial cell lines, HPL1D and BEAS2B, which confirmed CHGB induction at varying degrees in all 4 cell lines (Supplementary Fig. S2C).

To study the direct effects of *miR-375*, we analyzed changes in the expression profiles of target genes for *miR-375* predicted with TargetScan4.1 (http://www.targetscan.org/) and observed leftward shifts of the expression profile histograms, especially at 24 and 48 hours after *miR-375* transfection (Fig. 4A), which indicated moderate but significant downregulation of the predicted target genes of *miR-375*. In contrast, histograms of genes residing in chromosome 1 did not show any shifts, confirming specificity. Among the potential target genes affected by *miR-375*, transcriptional coactivator YAP1 was the most significantly repressed after *miR-375* transfection (Fig. 4B), which was also confirmed by Western blotting analysis (Fig. 4C). Two potential *miR-375* binding sites were also noted within the 3′-UTR of YAP1 mRNA, thus we carried out a luciferase assay by using YAP1 3′-UTR reporters (miR-375 × 1 and miR-375 × 2) containing either 1 or 2 potential *miR-375* binding sites (Fig. 4D). A549 cells transfected with these reporter constructs along with either Pre-miR-375 or negative control Pre-miR-NC#2 showed significant suppression of luciferase activity in a target site-dependent manner. The YAP1 3′-UTR reporter with deletion of the potential *miR-375* binding site abrogated *miR-375*–mediated suppression of luciferase activity (Supplementary Fig. S5A). The specificity of the *miR-375* target sites was also supported by our findings of lack of suppression of the wild-type YAP1 3′-UTR reporter activity by various unrelated miRNAs (Supplementary Fig. S5B). The relationship of *miR-375* with YAP1 was also substantiated by the significant negative correlation ($R = 0.793$, $P < 0.0001$) between *miR-375* and YAP1 in a panel of 29 lung cancer cell lines and 2 immortalized normal airway epithelial cell lines (Fig. 4E, left). In addition, we observed a histologic type-dependent expression pattern with low YAP1 expression in SCLC and abundant expression in NSCLC cell lines, indicating an expression pattern opposite to that of *miR-375*, which has abundant expression in SCLC (Fig. 4E, right). These relationships among ASH1, *miR-375*, and YAP1 were also observed in primary lung cancer specimens (Fig. 4F), suggesting the existence of robust regulatory relationships in the ASH1–*miR-375*–YAP1 pathway in lung cancers with NE features.

The negative correlation between *miR-375* and YAP1 found in a histologic type-related manner prompted us to investigate YAP1 functions in lung cancer cells of both histologic types. A549 adenocarcinoma and ACC-LC-172 SCLC cell lines were infected with YAP1-expressing or an empty lentivirus expressing the fluorescent protein Venus from an internal ribosomal entry site. Fluorescent microscopic examination revealed marked reduction of the fluorescence-positive population, which was indicative of successful infection by the YAP1-expressing virus, in contrast to robust growth in fluorescence-negative uninfected ACC-LC-172 cells (Fig. 5A), which we also confirmed by fluorescence-activated cell sorting analysis (Fig. 5B). In contrast to ACC-LC-172, A549 cells seemed to be tolerant to the introduction of YAP1, because the fluorescence-positive YAP1-infected population gradually increased (Fig. 5B). Time courses of fluorescent signals in lentivirus-infected A549 and ACC-LC172 cells are shown in Supplementary Figure S6A. YAP1-virus infection significantly inhibited the increase of fluorescent signals in ACC-LC-172 cells, but not in A549, suggesting a lineage-dependent growth-suppressive effect of YAP1. These findings were also confirmed by Western

Published OnlineFirst August 19, 2011; DOI:10.1158/0008-5472.CAN-11-1020

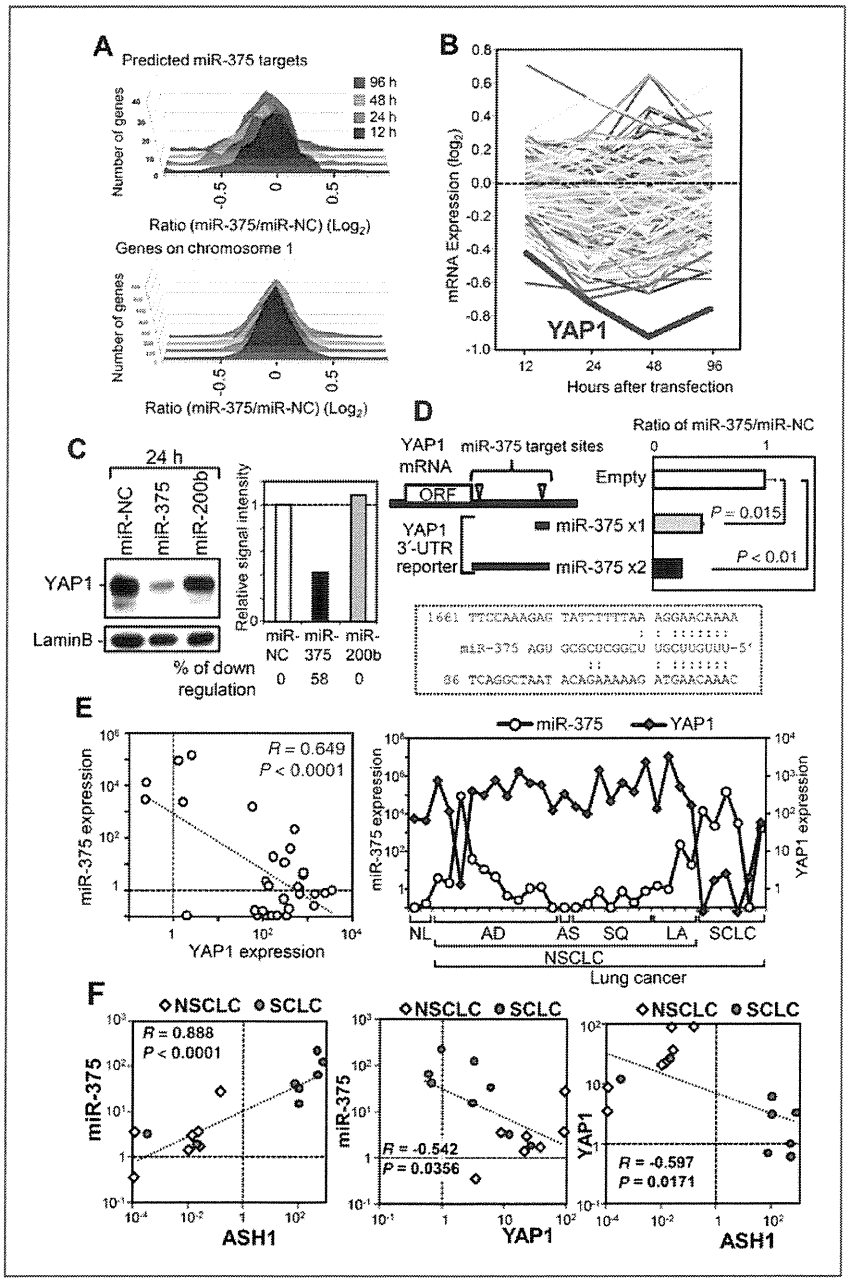

Figure 4. YAP1 inhibition by *miR-375*. A, histogram of gene expressions at 4 time points after Pre-miR-375 transfection. Gene expressions at 12 to 96 hours after transfection are shown as $\log_2$ ratio values between A549 cells transfected with Pre-miR-375 and Pre-miR-NC#2. Top, *miR-375* predicted target genes; bottom, genes residing in chromosome 1, which was used as a control. B, time course of expression of each *miR-375* predicted target gene after Pre-miR-375 transfection. C, Western blotting analysis of YAP1 protein. A549 cells transfected with Pre-miR-RNAs (15 nmol/L) were analyzed by Western blotting with the antibody against endogenous YAP1 protein. The intensity of YAP1 bands was determined with a densitometer and normalized with lamin B bands. Pre-miR-375 transfection downregulated the level of YAP1 protein by 58%. This downregulation is shown with a bar graph, in which the extent of downregulation is also numerically indicated. D, YAP1 3′-UTR reporter assay. YAP1 mRNA contains 2 *miR-375* target sites at the 3′-UTR. Two reporter constructs, miR-375 × 1 and miR-375 × 2, carry 1 and 2 *miR-375* sites, respectively. A549 cells were transfected with reporter constructs and Pre-miR-RNAs (10 nmol/L). The ratio of luciferase activity of Pre-miR-375 transfectants to that of Pre-miR-NC#2 transfectants is shown. *miR-375* significantly suppressed luciferase activity in a target site-dependent manner. The alignment of 2 *miR-375* target sites with mature *miR-375* is also shown. The nucleotide positions in 3′-UTR are indicated. E, negative correlations of *miR-375* and YAP1 expressions in lung cancer cell lines. Left, YAP1 and *miR-375* expressions showed significant negative correlations among the tested lung cancer cell lines. Right, YAP1 was frequently overexpressed in AD and SQ cells, whereas its expression was strongly suppressed in SCLC. In contrast, most SCLC showed overexpression of *miR-375*, whereas *miR-375* was scarcely expressed in the AD and SQ cell lines. F, correlations of ASH1, *miR-375*, and YAP1 expression levels in primary lung cancer specimens. ASH1 and *miR-375* expressions were positively correlated, whereas inverse correlations were present between *miR-375* and YAP1, as well as between ASH1 and YAP1. NL, normal lung; AD, adenocarcinoma; SQ, squamous cell carcinoma; LA, large cell carcinoma; AS, adenosquamous carcinoma.

Published OnlineFirst August 19, 2011; DOI:10.1158/0008-5472.CAN-11-1020

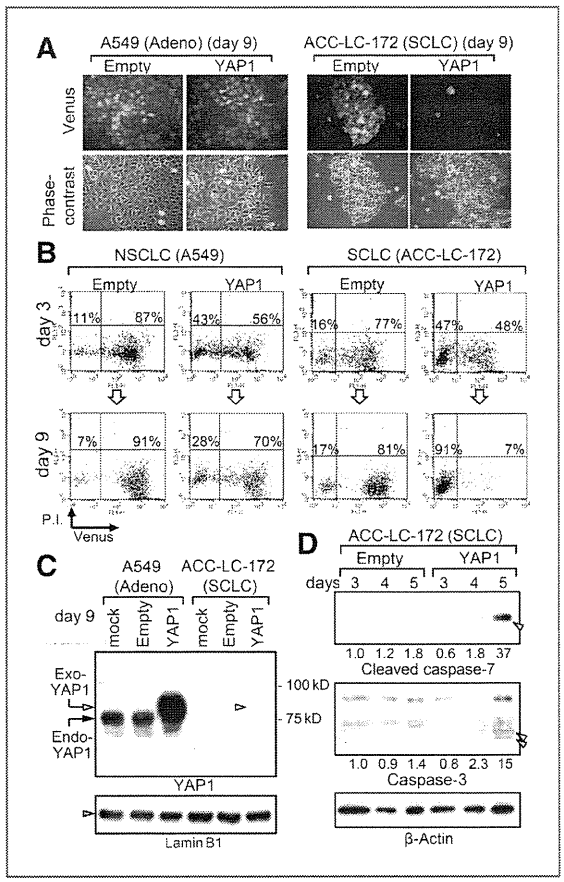

Figure 5. Lineage-dependent growth-regulating effects of YAP1 in lung cancers. A, fluorescent image of lentivirus-infected A549 and ACC-LC-172 obtained 9 days after infection. Cells were infected with a YAP1-expressing or empty lentivirus carrying the fluorescent protein Venus. YAP1 and empty virus infection resulted in fluorescent signals in A549 cells. In contrast, fluorescence-positive cells were scarcely detected in ACC-LC-172 cells infected with the YAP1-virus, whereas noninfected cells grew well. B, flow cytometric analysis of fluorescence-positive cells. Lentivirus-infected cells were analyzed at 3 and 9 days after infection. The fluorescence-positive population was moderately increased in the A549 cells infected with the YAP1-virus, whereas that population almost disappeared in ACC-LC-172 cells infected with the YAP1-virus. C, Western blotting analysis of YAP1. A549 abundantly expressed endogenous and exogenous (HA-tagged) YAP1. In contrast, ACC-LC-172 did not express endogenous YAP1. In addition, exogenous YAP1 was scarcely detected. D, Western blotting analysis of caspases. Five days after infection, activated cleavage of caspase-7 and caspase-3 was detected in YAP1 virus-infected ACC-LC-172 cells. Normalized intensities of cleaved caspases are numerically indicated.

blotting analysis, using lysates harvested on day 9, which showed scarcely detectable HA-tagged exogenous YAP1 protein expression in ACC-LC-172 as opposed to the abundant exogenous YAP1 expression in A549 cells (Fig. 5C). Cleavage of caspase-7 and caspase-3 was detected in YAP1-introduced ACC-LC-172 cells (Fig. 5D), whereas propidium iodide–stained dead cells were frequently observed in YAP1-introduced fluorescence-positive cells in ACC-LC-172 (Supplementary Fig. S6B), but not in A549 (data not shown). YAP1 introduction also resulted in growth suppression in 2 other SCLC cell lines, NCI-H69 and ACC-LC-48 (Supplementary Fig. S7), which confirmed the results observed in ACC-LC-172.

Discussion

The present results clearly show that ASH1 directly transactivates *miR-375*, resulting in an NE lineage-specific upregulation of *miR-375* in lung cancers. Although NeuroD1 and Pdx1 potentially bind to the E-box in the *miR-375* promoter (13), their expression was rarely detected and showed no correlations with *miR-375* expression (data not shown). Therefore, we believe that ASH1 plays a major role as a transcriptional activator of *miR-375*. Our finding of NEB-specific expression of *miR-375* also supports the existence of an ASH1–*miR-375* signaling axis in the lung. It is important to note that *miR-375* was recently reported to be detectable in pancreatic islet cells under the regulation of NeuroD1 and Pdx1, as well as in pituitary and adrenal glands (13–16). Herein, we clearly showed the functional importance of 3 E-boxes (E1, E2, and E3) in ASH1-mediated induction of the promoter activity of *miR-375*. Furthermore, a recent report described the promoter activity of a similar genomic region 5′ to murine *miR-375* in a β-cell line, though its responsiveness to potential activators such as NeuroD1 and ASH1 was not examined (17).

Downregulation of *miR-375* has been reported in a few other types of cancer (18–20). Interestingly, *miR-375* was suggested to play tumor suppressor roles in those cancer types, whereas target genes for *miR-375* thus far reported include PDK1, 14-3-3ζ (19), HuD (21), and JAK2 (22). Also, hepatocellular carcinoma was recently added to the list of cancers with *miR-375* downregulation and YAP1 has been suggested to be a target gene relieved by that downregulation. Consistent with those findings, we observed moderate downregulation of PDK1, 14-3-3ζ, HuD, and JAK2 when *miR-375* was introduced to A549 cells, though YAP1 showed the most significant downregulation in our experimental settings (Supplementary Fig. S8B). In addition, we did not observe clear growth inhibition of A549 cells stably introduced with a lentivirus expressing *miR-375* (Supplementary Fig. S8A), even though YAP1 was effectively downregulated by *miR-375* (Fig. 4B–D). Along this line, it is notable that *miR-375* knockout mice were shown to be hyperglycemic in association with decreased β-cell mass as a result of impaired proliferation of β-cells (15) and that *miR-375* was shown to regulate a number of genes other than *YAP1*, which potentially control cellular growth and proliferation of pancreatic islets (15). It is also interesting that estrogen receptor-α (ERα)-expressing breast cancers showed ERα-signal dependency and a high expression of *miR-375* (23). ERα binds the *miR-375* promoter and induces its expression. *miR-375* in turn represses the *RAS, dexamethasone-induced 1* (*RASD1*) gene, which negatively regulates ERα expression, suggesting the existence of a positive feedback loop between ERα and *miR-375*, as well as a growth-promoting role of *miR-375* in ERα-positive breast cancers (23). Taken together, it is conceivable that *miR-375* plays distinct roles in various can-

Published OnlineFirst August 19, 2011; DOI:10.1158/0008-5472.CAN-11-1020

cers, depending on the cellular context and transcriptomes including its potential target genes, and that downregulation of YAP1 by ASH-1-transactivated *miR-375* promotes rather than inhibits growth of SCLC cells.

YAP1 has several domains including a TEAD binding region and 2 WW domains, whereas it lacks a DNA binding domain and functions as a transcriptional coactivator through interactions with DNA binding transcription factors (24–26). YAP1 interacts with the TEAD family through a TEAD binding domain, and transactivates growth-promoting genes, whereas it also binds to PPXY motif-containing molecules including p73 through WW domains, thus enhancing p73-dependent apoptosis in response to DNA damage (27–29). It has been reported that phosphorylation by AKT or repression by ΔNp63 downregulates the proapoptotic activity of YAP1 (30), and that PML is also involved in regulation of p73-YAP apoptotic signaling through sumoylation and stabilization of YAP (31). Therefore, accumulating evidence enhances the notion that YAP1 exerts both oncogenic and tumor-suppressive activities in a context-dependent manner (32, 33). The present findings show that YAP1 moderately promotes NSCLC proliferation when overexpressed, whereas it significantly suppresses SCLC growth, suggesting its lineage-dependent dual roles in lung cancers.

In conclusion, we identified *miR-375* as a direct transcriptional target for ASH1 and showed that it has a crucial role for mediating signals required for ASH1-mediated induction of NE features in lung cancers. In addition, the present findings indicate that *miR-375* directly downregulates YAP1, whereas we also found that it shows NE lineage-specific growth inhibitory activities in lung cancers. A future study of the downstream genes of the ASH1–*miR-375* axis will be of great interest to fully elucidate the underlying signaling networks involved in NE differentiation and highly malignant behaviors of NE lung cancers including SCLC.

Disclosure of Potential Conflicts of Interest

No potential conflicts of interest were disclosed.

Acknowledgments

We thank Dr. Hideki Murakami and Ms. Mika Yamamoto for their excellent technical help. We also thank Dr. H. Miyoshi (RIKEN BioResource Center) and Dr. A. Miyawaki (RIKEN Brain Science Institute) for generously providing the lentivirus vectors and Venus gene, respectively.

Grant Support

This work was supported in part by Grants-in-Aid for Scientific Research on Priority Areas and Scientific Research on Innovative Areas from the Ministry of Education, Culture, Sports, Science and Technology (MEXT) of Japan; grants-in-aid for Scientific Research (A) and (C) from the Japan Society for the Promotion of Science (JSPS); and grants-in-aid for Scientific Research from the Princess Takamatsu Cancer Research Fund, the Uehara Memorial Foundation and the Nagono Medical Foundation. E.Nishikawa was supported by a JSPS Research Fellowship.

The costs of publication of this article were defrayed in part by the payment of page charges. This article must therefore be hereby marked *advertisement* in accordance with 18 U.S.C. Section 1734 solely to indicate this fact.

Received March 23, 2011; revised August 4, 2011; accepted August 12, 2011; published OnlineFirst August 19, 2011.

References

1. Takahashi T, Sidransky D. Biology of lung cancer. In:Mason R, Broaddus V, Murray J, Nadel J, editors. Textbook of respiratory medicine. 4th ed. Philadelphia, PA: Elsevier Science; 2005. p. 1311–27.
2. Voortman J, Goto A, Mendiboure J, Sohn JJ, Schetter AJ, Saito M, et al. MicroRNA expression and clinical outcomes in patients treated with adjuvant chemotherapy after complete resection of non-small cell lung carcinoma. Cancer Res 2010;70:8288–98.
3. Du L, Schageman JJ, Irnov , Girard L, Hammond SM, Minna JD, et al. MicroRNA expression distinguishes SCLC from NSCLC lung tumor cells and suggests a possible pathological relationship between SCLCs and NSCLCs. J Exp Clin Cancer Res 2010;29:75.
4. Osada H, Takahashi T. MicroRNAs in biological processes and carcinogenesis. Carcinogenesis 2007;28:2–12.
5. Osada H, Takahashi T. let-7 and miR-17-92: small-sized major players in lung cancer development. Cancer Sci 2011;102:9–17.
6. Takamizawa J, Konishi H, Yanagisawa K, Tomida S, Osada H, Endoh H, et al. Reduced expression of the let-7 microRNAs in human lung cancers in association with shortened postoperative survival. Cancer Res 2004;64:3753–6.
7. Hayashita Y, Osada H, Tatematsu Y, Yamada H, Yanagisawa K, Tomida S, et al. A polycistronic microRNA cluster, miR-17-92, is overexpressed in human lung cancers and enhances cell proliferation. Cancer Res 2005;65:9628–32.
8. Matsubara H, Takeuchi T, Nishikawa E, Yanagisawa K, Hayashita Y, Ebi H, et al. Apoptosis induction by antisense oligonucleotides against miR-17-5p and miR-20a in lung cancers overexpressing miR-17-92. Oncogene 2007;26:6099–105.
9. Osada H, Tomida S, Yatabe Y, Tatematsu Y, Takeuchi T, Murakami H, et al. Roles of achaete-scute homologue 1 in DKK1 and E-cadherin repression and neuroendocrine differentiation in lung cancer. Cancer Res 2008;68:1647–55.
10. Osada H, Tatematsu Y, Yatabe Y, Horio Y, Takahashi T. ASH1 gene is a specific therapeutic target for lung cancers with neuroendocrine features. Cancer Res 2005;65:10680–5.
11. Dutta KK, Zhong Y, Liu YT, Yamada T, Akatsuka S, Hu Q, et al. Association of microRNA-34a overexpression with proliferation is cell type-dependent. Cancer Sci 2007;98:1845–52.
12. Linnoila RI. Functional facets of the pulmonary neuroendocrine system. Lab Invest 2006;86:425–44.
13. Keller DM, McWeeney S, Arsenlis A, Drouin J, Wright CV, Wang H, et al. Characterization of pancreatic transcription factor Pdx-1 binding sites using promoter microarray and serial analysis of chromatin occupancy. J Biol Chem 2007;282:32084–92.
14. Kapsimali M, Kloosterman WP, de Bruijn E, Rosa F, Plasterk RH, Wilson SW. MicroRNAs show a wide diversity of expression profiles in the developing and mature central nervous system. Genome Biol 2007;8:R173.
15. Poy MN, Hausser J, Trajkovski M, Braun M, Collins S, Rorsman P, et al. miR-375 maintains normal pancreatic alpha- and beta-cell mass. Proc Natl Acad Sci U S A 2009;106:5813–8.
16. Baroukh NN, Van Obberghen E. Function of microRNA-375 and microRNA-124a in pancreas and brain. FEBS J 2009;276:6509–21.
17. Avnit-Sagi T, Kantorovich L, Kredo-Russo S, Hornstein E, Walker MD. The promoter of the pri-miR-375 gene directs expression selectively to the endocrine pancreas. PLoS One 2009;4:e5033.
18. Mathe EA, Nguyen GH, Bowman ED, Zhao Y, Budhu A, Schetter AJ, et al. MicroRNA expression in squamous cell carcinoma and

Published OnlineFirst August 19, 2011; DOI:10.1158/0008-5472.CAN-11-1020

adenocarcinoma of the esophagus: associations with survival. Clin Cancer Res 2009;15:6192–200.

19. Tsukamoto Y, Nakada C, Noguchi T, Tanigawa M, Nguyen LT, Uchida T, et al. MicroRNA-375 is downregulated in gastric carcinomas and regulates cell survival by targeting PDK1 and 14-3-3zeta. Cancer Res 2010;70:2339–49.
20. Liu AM, Poon RT, Luk JM. MicroRNA-375 targets Hippo-signaling effector YAP in liver cancer and inhibits tumor properties. Biochem Biophys Res Commun 2010;394:623–7.
21. Abdelmohsen K, Hutchison ER, Lee EK, Kuwano Y, Kim MM, Masuda K, et al. miR-375 inhibits differentiation of neurites by lowering HuD levels. Mol Cell Biol 2010;30:4197–210.
22. Ding L, Xu Y, Zhang W, Deng Y, Si M, Du Y, et al. MiR-375 frequently downregulated in gastric cancer inhibits cell proliferation by targeting JAK2. Cell Res 2010;20:784–93.
23. de Souza Rocha Simonini P, Breiling A, Gupta N, Malekpour M, Youns M, Omranipour R, et al. Epigenetically deregulated microRNA-375 is involved in a positive feedback loop with estrogen receptor alpha in breast cancer cells. Cancer Res 2010;70:9175–84.
24. Wang K, Degerny C, Xu M, Yang XJ. YAP, TAZ, and Yorkie: a conserved family of signal-responsive transcriptional coregulators in animal development and human disease. Biochem Cell Biol 2009; 87:77–91.
25. Bertini E, Oka T, Sudol M, Strano S, Blandino G. YAP: at the crossroad between transformation and tumor suppression. Cell Cycle 2009;8: 49–57.
26. Zhao B, Li L, Lei Q, Guan KL. The Hippo-YAP pathway in organ size control and tumorigenesis: an updated version. Genes Dev 2010;24: 862–74.
27. Strano S, Munarriz E, Rossi M, Castagnoli L, Shaul Y, Sacchi A, et al. Physical interaction with Yes-associated protein enhances p73 transcriptional activity. J Biol Chem 2001;276:15164–73.
28. Oka T, Mazack V, Sudol M. Mst2 and Lats kinases regulate apoptotic function of Yes kinase-associated protein (YAP). J Biol Chem 2008;283:27534–46.
29. Oka T, Sudol M. Nuclear localization and pro-apoptotic signaling of YAP2 require intact PDZ-binding motif. Genes Cells 2009;14: 607–15.
30. Ehsanian R, Brown M, Lu H, Yang XP, Pattatheyil A, Yan B, et al. YAP dysregulation by phosphorylation or DeltaNp63-mediated gene repression promotes proliferation, survival and migration in head and neck cancer subsets. Oncogene 2010;29:6160–71.
31. Lapi E, Di Agostino S, Donzelli S, Gal H, Domany E, Rechavi G, et al. PML, YAP, and p73 are components of a proapoptotic autoregulatory feedback loop. Mol Cell 2008;32:803–14.
32. Yuan M, Tomlinson V, Lara R, Holliday D, Chelala C, Harada T, et al. Yes-associated protein (YAP) functions as a tumor suppressor in breast. Cell Death Differ 2008;15:1752–9.
33. Zhang H, Pasolli HA, Fuchs E. Yes-associated protein (YAP) transcriptional coactivator functions in balancing growth and differentiation in skin. Proc Natl Acad Sci U S A 2011;108: 2270–5.